transactivation of its downstream signals involving transcription factors and cell cycle regulators.

Materials and Methods

Cell lines and clinical tissue samples. The 19 human lung cancer cell lines used in this study were as follows: 15 NSCLCs—A549, NCI-H23, NCI-H358, NCI-H522, NCI-H1435, NCI-H1793, LC174, LC176, LC319, PC3, PC9, PC14, SK-LU-1, RERF-LC-AI, and SK-MES-1; and 4 small cell lung cancers (SCLC)—SBC-3, SBC-5, DMS114, and DMS273. All cells were grown in the appropriate medium supplemented with 10% FCS and were maintained at 37°C in an atmosphere of humidified air with 5% CO_2.

Primary NSCLC samples had been obtained earlier with informed consent from 37 patients (4). Fifteen additional primary NSCLCs, including seven adenocarcinomas and eight squamous cell carcinomas, were obtained along with adjacent normal lung tissue samples from patients undergoing surgery at Hokkaido University and its affiliated hospitals (Sapporo, Japan).

A total of 326 formalin-fixed primary NSCLCs (stage I-IIIa) including 224 adenocarcinomas, 86 squamous cell carcinomas, 13 large-cell carcinomas, and 3 adenosquamous carcinomas, and adjacent normal lung tissue samples were obtained from patients who underwent surgery at Hokkaido University and its affiliated hospitals (Sapporo, Japan), and Saitama Cancer Center (Saitama, Japan). Large cell neuroendocrine carcinoma samples from three patients were obtained from the Saitama Cancer Center. Samples of advanced SCLC (stage IV) from postmortem materials (17 individuals) obtained from Hiroshima University (Hiroshima, Japan), were also used in this study. The use of all clinical materials was approved by the Institutional Research Ethics Committees.

Semiquantitative reverse transcription-PCR analysis. Total RNA was extracted from cultured cells and clinical tissues using Trizol reagent (Life Technologies, Inc., Gaithersburg, MD) according to the manufacturer's protocol. Extracted RNAs and normal human tissue polyadenylate RNAs were treated with DNase I (Nippon Gene, Tokyo, Japan) and were reverse-transcribed using oligo$(dT)_{20}$ primer and SuperScript II reverse transcriptase (Invitrogen, Carlsbad, CA). Semiquantitative reverse transcription-PCR (RT-PCR) experiments were carried out with the following synthesized gene-specific primers or with β-actin (*ACTB*)-specific primers as an internal control: *NMU*, 5′-TGAAGAGATTCAGAGTGGACGA-3′ and 5′-ACTGAGAACATTGACAACACAGG-3′; *NMU1R*, 5′-AAGAGGGACAGGGACAAGTAGT-3′ and 5′-ATGCCACTGTTACTGCTTCAG-3′; *NMU2R*, 5′-GGCTCTTACAACTCATGTACCCA-3′ and 5′-TGATACAGAGACATGAAGTGAGCA-3′; *GHSR1a*, 5′-TGGTGTTTGCCTTCATCCT-3′ and 5′-GAATCCCAGAAGTCTGAACA-3′; *GHSR1b*, 5′-CTTGGGACACCAACGAGTG-3′ and 5′-AGGACCCGCGAGAGAAAGC-3′; *NTSR1*, 5′-GGTCTGTGGCTGTGACTGAA-3′ and 5′-GTTTGAGCTGTGAGGGCTGT-3′; *GHRL*, 5′-TGAGCCCTGAACACCAGAGAG-3′ and 5′-AAAGCCAGATGAGCGCTTCTA-3′; *NTS*, 5′-TCTTCAGCATGATGTGTTGTGT-3′ and 5′-TGAGAGATTCATGAGGAAGTCTTG-3′; *FOXM1*, 5′-CCCTGACAACATCAACTGGTC-3′ and 5′-GTCCACCTTCGCTTTTATTGAGT-3′; unannotated transcript (clone IMAGE:3839141, mRNA), 5′-AAAAAGGGGATGCCTAGAACTC-3′ and 5′-CTTTCAGCACGTCAAGGACAT-3′; *GCDH*, 5′-ACACCTACGAAGGTACACATGAC-3′ and 5′-GCTATTTCAGGGTAAATGGAGTC-3′; *CDK5RAP1*, 5′-CAGAGATGGAGGATGTCAATAAC-3′ and 5′-CATAGCAGCTTTAAAGAGACACG-3′; *LOC134145*, 5′-CCACCATAACAGTGGAGTGGG-3′ and 5′-CAGTTACAGGTGTATGACTGGGAG-3′; *NUP188*, 5′-CTGAATACAACTTCCTGTTTGCC-3′ and 5′-GACCACAGAATTACCAAAACTGC-3′; *ACTB*, 5′-GAGGTGATAGCATTGCTTTCG-3′ and 5′-CAAGTCAGTGTACAGGTAAGC-3′. PCR reactions were optimized for the number of cycles to ensure product intensity within the logarithmic phase of amplification.

Northern blot analysis. Human multiple-tissue blots (BD Biosciences Clontech, Palo Alto, CA) were hybridized with a ^{32}P-labeled PCR product of *NMU*. The full-length cDNA of *NMU* was prepared by RT-PCR using primers 5′-CGCGGATCCGCGATGCTGCGAACAGAGAGCTG-3′ and 5′-CCGCTCGAGCGGAATGAACCCTGCTGACCTTC-3′. Prehybridization, hybridization, and washing were done according to the supplier's recommendations. The blots were autoradiographed with intensifying screens at room temperature for 72 hours.

Western blotting. Cells were lysed with radioimmunoprecipitation assay buffer [50 mmol/L Tris-HCl (pH 8.0), 150 mmol/L NaCl, 1% NP40, 0.5% deoxychorate-Na, 0.1% SDS] containing Protease Inhibitor Cocktail Set III (Calbiochem, Darmstadt, Germany). Protein samples were separated by SDS-polyacrylamide gels and electroblotted onto Hybond-ECL nitrocellulose membranes (GE Healthcare Bio-Sciences, Piscataway, NJ). Blots were incubated with a rabbit polyclonal anti-NMU antibody (generated to recombinant NMU), mouse monoclonal anti-FLAG M2 antibody (Sigma-Aldrich, Co., St. Louis, MO), goat polyclonal anti-NTSR1 antibody (Santa Cruz Biotechnology, Inc., Santa Cruz, CA), and rabbit polyclonal anti-GHSR antibody (generated to the peptide GVEHENGTDPWDTNEC). Antigen-antibody complexes were detected using secondary antibodies conjugated to horseradish peroxidase (GE Healthcare Bio-Sciences). Protein bands were visualized by enhanced chemiluminescence Western blotting detection reagents (GE Healthcare Bio-Sciences).

Immunohistochemistry and tissue microarray. To investigate the presence of NMU, GHSR1b, NTSR1, or FOXM1 protein in clinical samples (normal lung tissues, NSCLCs, and SCLCs that had been embedded in the paraffin block), we stained the sections using ENVISION+ Kit/horseradish peroxidase (DakoCytomation, Glostrup, Denmark). Briefly, each polyclonal antibody to NMU, GHSR1b (generated to the peptide GGSQRALRLSLAGPILSLC), NTSR1, or FOXM1 (Santa Cruz Biotechnology) was added after blocking endogenous peroxidase and proteins, and the sections were incubated with horseradish peroxidase–labeled anti-rabbit IgG and anti-goat IgG as the secondary antibody. Substrate chromogen was added and the specimens were counterstained with hematoxylin.

The tumor tissue microarrays were constructed as published previously (20, 21). The tissue area for sampling was selected based on a visual alignment with the corresponding H&E-stained section on a slide. Three-, four-, or five-tissue cores (diameter, 0.6 mm; height, 3-4 mm) taken from the donor tumor blocks were placed into a recipient paraffin block using a tissue microarrayer (Beecher Instruments, Sun Prairie, WI). A core of normal tissue was punched from each case. Five-micrometer sections of the resulting microarray block were used for immunohistochemical analysis. NMU positivity was assessed according to staining intensity as absent (no visible staining in tumor cells) or positive (dark brown staining in >50% of tumor cells completely obscuring cytoplasm) by three independent investigators without prior knowledge of the clinical follow-up data. The intensity of GHSR1b or NTSR1 staining was evaluated as well using the following criteria: positive, dark brown staining in >50% of tumor cells completely obscuring membrane and cytoplasm; absent, no appreciable staining in tumor cells. The intensity of FOXM1 staining was evaluated using the following criteria: positive, dark brown staining in >50% of tumor cells completely obscuring nucleus and cytoplasm; absent, no appreciable staining in tumor cells. Cases were accepted only as positive if reviewers independently defined them as such.

Statistical analysis. Tumor-specific survival curves were calculated from the date of surgery to the time of death related to NSCLC, or to the last follow-up observation. Kaplan-Meier curves were calculated for each relevant variable; differences in survival times among patient subgroups were analyzed using the log-rank test. Univariate and multivariate analyses were done using Cox's proportional hazard regression model to determine associations between clinicopathologic variables and cancer-related mortality. $P < 0.05$ were considered statistically significant.

Immunocytochemical analyses. Cultured cells were washed twice with PBS(−), fixed in 4% paraformaldehyde solution for 60 minutes at room temperature, and rendered permeable with PBS(−) containing 0.1% Triton X-100 for 1.5 minutes. Prior to the primary antibody reaction, cells were covered with blocking solution (3% bovine serum albumin (BSA) in PBS(−)) for 60 minutes to block nonspecific antibody binding. Then the cells were incubated with antibodies to human NMU protein. Antibodies were stained with a goat anti-rabbit secondary antibody conjugated to rhodamine (Cappel, Durham, NC) for revealing endogenous NMU, and viewed with a microscope (DP50; Olympus, Tokyo, Japan).

RNA interference assay. We had previously established a vector-based RNA interference (RNAi) system, psiH1BX3.0, to direct the synthesis of short interfering RNAs (siRNA) in mammalian cells (6, 7, 10, 11). We transfected

10 μg of siRNA expression vector, using 30 μL of LipofectAMINE 2000 (Invitrogen), into NSCLC cell lines A549 and LC319, both of which overexpressed *NMU, GHSR1b, NTSR1*, and *FOXM1* endogenously. The transfected cells were cultured for 5 days in the presence of appropriate concentrations of geneticin (G418), after which, cell numbers and viability were measured by Giemsa staining and triplicate 3-(4,5-dimethylthiazol-2-yl)-2,5-diphenyltetrazolium bromide (MTT) assays. The target sequences of the synthetic oligonucleotides for RNAi were as follows: control 1 [*EGFP*: enhanced green fluorescent protein gene, a mutant of *Aequorea victoria* green fluorescent protein], 5′-GAAGCAGCACGACTTCTTC-3′; control 2 (Luciferase: *Photinus pyralis* luciferase gene), 5′-CGTACGCGGAATACTTCGA-3′; control 3 (Scramble: chloroplast *Euglena gracilis* gene coding for 5S and 16S rRNAs), 5′-GCGCGCTTTGTAGGATTCG-3′; siRNA-NMU (si-*NMU*), 5′-GAGATTCAGAGTGGACGAA-3′; siRNA-GHSR-1 (si-*GHSR-1*), 5′-CCTCTACCTGTCCAGCATG-3′; siRNA-GHSR-2 (si-*GHSR-2*), 5′-GCTGGTCATCTTCGTCATC-3′; siRNA-NTSR1-1 (si-*NTSR1-1*), 5′-GTTCATCAGCGCCATCTGG-3′; siRNA-NTSR1-2 (si-*NTSR1-2*), 5′-GGTCGTCATACAGGTCAAC-3′. To validate our RNAi system, individual control siRNAs (EGFP, Luciferase, and Scramble) were initially confirmed using semiquantitative RT-PCR to decrease the expression of the corresponding target genes that had been transiently transfected into COS-7 cells. Down-regulation of *NMU, GHSR1b*, and *NTSR1* expression by their respective siRNAs (si-*NMU*, si-*GHSR-1*, si-*NTSR1-1*, and si-*NTSR1-2*), but not by controls, was confirmed with semiquantitative RT-PCR in the cell lines used for this assay.

NMU-expressing COS-7 transfectants. NMU-expressing stable transfectants were established according to a standard protocol. The entire coding region of *NMU* was amplified by RT-PCR using the primer sets described above. The product was digested with *Bam*HI and *Xho*I, and cloned into appropriate sites of a pcDNA3.1-myc/His A(+) vector (Invitrogen) that contained c-myc-His-epitope sequences (LDEESILKQEHHHHHH) at the COOH-terminal of the NMU protein. Using FuGENE 6 Transfection Reagent (Roche Diagnostics, Basel, Switzerland) according to the manufacturer's instructions, we transfected COS-7 cells, which do not express endogenous NMU, with plasmids expressing either *NMU* (pcDNA3.1-*NMU*-myc/His), an antisense strand of *NMU* (pcDNA3.1-antisense), or mock plasmids (pcDNA3.1). Transfected cells were cultured in DMEM containing 10% FCS and geneticin (0.4 mg/mL) for 14 days; then 50 individual colonies were trypsinized and screened for stable transfectants by a limiting-dilution assay. Expression of NMU was determined in each clone by RT-PCR, Western blotting, and immunostaining.

Cell growth and colony formation assays. COS-7 transfectants that stably expressed NMU were seeded onto six-well plates (5×10^4 cells/well), and maintained in medium containing 10% FCS and 0.4 mg/mL geneticin for 24, 48, 72, 96, 120, and 144 hours. At each time point, cell proliferation was evaluated by the MTT assay using Cell Counting Kits (Wako, Osaka, Japan). Colonies were counted at 144 hours. All experiments were done in triplicate. Interaction of NMU-25 with COS-7 cells were examined by flow cytometric analysis. Briefly, subconfluent cells were harvested in Cell Dissociation Solution (Sigma-Aldrich) and suspended in DMEM. Then, 1×10^6 cells/microtube were washed with assay buffer [PBS(−) with 10 mmol/L $MgCl_2$, 2 mmol/L EDTA, and 0.1% BSA], and the cells were incubated with 0.5 to 10 μmol/L of rhodamine-labeled NMU-25 peptide (NMU-25-rhodamine; Phoenix Pharmaceuticals, Inc., Belmont, CA) in assay buffer for 2 hours at room temperature. Subsequently, the cells were washed twice with assay buffer. To detect the population of cells binding to rhodamine-labeled NMU-25, flow cytometry was done using a Becton Dickinson FACSCalibur and analyzed by Cell Quest software.

Ligand receptor binding assay. To confirm binding of NMU-25 to the endogenous candidate receptors on the NSCLC cells, we did a receptor-ligand binding assay using the LC319 and PC14 cells that expressed GHSR1b and NTSR1, but did not express NMU1R and NMU2R. Briefly, the trypsinized cells were seeded onto 96-well (with a black wall and clear bottom) microtiter plates 24 hours prior to the assay. The medium was removed and the cells were incubated with Cy5-labeled NMU-25 peptide (1 μmol/L) with or without a 10-fold excess of unlabeled NMU-25 peptide as a competitor. The plate was incubated in the dark for 24 hours at 37°C and was then scanned on the 8200 Cellular Detection System (Applied Biosystems, Foster City, CA) to quantify the amount of Cy5 fluorescence probe bound to the surface of each cell.

Immunocytochemistry for internalized receptors. To investigate the association of NMU-25 with its candidate receptors, GHSR1b and NTSR1, we did the following experiments. The entire coding region of each receptor gene was amplified by RT-PCR using primers *GHSR1b* (5′-GGAATTCCATGTGGAACGCGACGCCCAGCGAA-3′ and 5′-CGCGGATCCGCGGAGAGAAGGGAGAAGGCACAGGGA-3′) and *NTSR1* (5′-GGAATTCCATGCGCCTCAACAGCTCCGCGCCGGGAA-3′ and 5′-CGCGGATCCGCGGTACAGCGTCTCGCGGGTGGCATTGCT-3′). The products were digested with *Eco*RI and *Bam*HI and cloned into appropriate sites of p3XFLAG-CMV10 vector (Sigma-Aldrich). We transfected COS-7 cells with FLAG-tagged GHSR1b or NTSR1 expression plasmids using FuGENE 6 Transfection Reagent, as described above. The cells subjected to internalization assays were exposed to NMU-25 (10 μmol/L) for 120 minutes. Cells were then fixed with 4% paraformaldehyde solution for 15 minutes at 37°C, and washed with PBS(−). Specimens were incubated in PBS(−) containing 0.1% Triton X-100 for 10 minutes and subsequently washed with PBS(−). Prior to the primary antibody reaction, cells were incubated in CAS-BLOCK (Zymed Laboratories, Inc., South San Francisco, CA) for 10 minutes to block nonspecific antibody binding. Then the cells were incubated with both rabbit polyclonal anti-GHSR antibody and goat polyclonal anti-NTSR1 antibody. Antibodies were stained with both anti-rabbit secondary antibody conjugated to Alexa Fluor 488 (Molecular Probes, Eugene, OR) and anti-goat secondary antibody conjugated to Alexa Fluor 594 (Molecular Probes). DNA was stained with 4′,6-diamidino-2-phenylindole (DAPI). Images were viewed and assessed using a confocal microscopy (TCS SP2 AOBS; Leica Microsystems, Wetzlar, Germany).

Internalization study with fluorescence ligand of NMU. LC319 cells were grown in DMEM containing 10% FCS. The cells were washed in PBS(−), and preincubated for 10 minutes at 37°C in DMEM containing 0.1% BSA. They were then incubated for various periods of time with Alexa Fluor 594–labeled NMU-25 peptide in DMEM containing 0.1% BSA. At the end of the incubation, the cells were washed thrice with ice-cold PBS(−), fixed with 4% paraformaldehyde solution, initially for 5 minutes on ice, and then for 15 minutes at room temperature. The cells were washed and treated with DAPI. Images were viewed and assessed using a confocal microscopy (TCS SP2 AOBS; Leica Microsystems). Optical sections with intervals of 0.25 μm were taken with a 63×/1.4 objective.

Detection of receptor dimerization. Cultured cells were washed twice with ice-cold PBS(−) and incubated with 5 mmol/L dithiobis[succinimidyl-propionate] (Pierce, Rockford, IL) for 60 minutes in PBS(−) on ice. The reaction was quenched by incubation with Stop solution [1 mol/L Tris (pH 7.5)] in a final concentration of 50 mmol/L Tris for 15 minutes on ice. Cells were then washed twice with ice-cold PBS(−) and lysed in ice-cold Tx/G buffer [300 mmol/L NaCl, 1% Triton X-100, 10% glycerol, 1.5 mmol/L $MgCl_2$, 1 mmol/L $CaCl_2$, and 10 mmol/L iodoacetamide in 50 mmol/L Tris-Cl (pH 7.4)] containing protease inhibitor (Protease Inhibitor Cocktail Set III; Calbiochem) for 60 minutes on ice. Iodoacetamide was included in each buffer used for protein preparation to prevent nonspecific disulfide linkages. The lysates were then centrifuged for 15 minutes at 15,000 rpm at 4°C, and the supernatants were incubated with anti-FLAG M2-agarose affinity beads (Sigma-Aldrich) at 4°C overnight. The immunoprecipitates (containing cell surface receptors) were collected, washed thrice with TBST buffer [150 mmol/L NaCl, 0.05% Tween 20 in 20 mmol/L Tris-Cl (pH 7.6)], and eluted in non–reducing Laemmli sample buffer. The solutions were subjected to SDS-PAGE, and receptor proteins were detected by Western blot analysis using a mouse monoclonal anti-FLAG M2 antibody, goat polyclonal anti-NTSR1 antibody, or rabbit polyclonal anti-GHSR antibody as a primary antibody, and rec-Protein G-Peroxidase Conjugate (Zymed Laboratories) to detect antigen-antibody complexes.

Measurement of cyclic AMP levels. Trypsinized LC319 cells were seeded onto 96-well microtiter plate (5.0×10^4 cells) and cultured in appropriate medium supplemented with 10% FCS for 24 hours, and then the medium was changed to serum-free/1 mmol/L of 3-isobutyl-1-methylxanthine 20 minutes prior to the assay. Next, cells were incubated with individual concentrations of peptides (NMU-25, GHRL, or NTS) for

20 minutes and their cyclic AMP (cAMP) levels were measured using the cAMP EIA System (GE Healthcare Bio-Sciences).

Identification of downstream genes of NMU by cDNA microarray. LC319 cells were transfected with either siRNA against *NMU* (si-*NMU*) or Luciferase (LUC; control siRNA). mRNAs were extracted 0, 6, 12, 24, 36, 48, and 60 hours after the transfection, labeled with Cy5 or Cy3 dye, and subjected to cohybridization onto cDNA microarray slides containing 32,256 genes as described (5). After normalization of the data, genes with signals higher than the cutoff value were analyzed further. Genes whose intensity was significantly decreased in accordance with the reduction of *NMU* expression were initially selected using self-organizing map cluster analysis (22). Validation of candidate downstream genes of NMU was done using semiquantitative RT-PCR experiments of the same mRNAs from LC319 cells used for microarray hybridization, with gene-specific primers.

Results

NMU in lung tumors and normal tissues. To search for novel target molecules for the development of therapeutic agents and/or diagnostic biomarkers for NSCLC, we first screened genes that showed 5-fold higher expression in >50% of 37 NSCLCs analyzed by cDNA microarray. Among the 23,040 genes screened, we identified the *NMU* transcript to be frequently overexpressed in these NSCLCs and confirmed increased *NMU* expression in the majority of additional NSCLC cases (Fig. 1*A*). In addition, we observed the up-regulation of *NMU* in 13 of 15 NSCLC cell lines and in all 4 SCLC cell lines examined (Fig. 1*B*). Using immunoblot analyses, we subsequently confirmed the expression of NMU protein in lung cancer tissues and cell lines. Western blot analysis revealed an increased NMU protein expression in tumor tissues from the representative pairs of NSCLC samples analyzed (Supplementary Fig. S1*A*). We also found increased NMU protein expression in lung cancer cell lines (Supplementary Fig. S1*B*); the results were consistent with the RT-PCR data (Fig. 1*B*). Northern blotting with *NMU* cDNA as a probe identified a 0.8 kb transcript as a very weak band only in brain and stomach among the 15 normal human tissues examined (data not shown). We also examined NMU expression in clinical lung cancers using tissue microarray system. Positive staining (dark brown staining in >50% of tumor cells completely obscuring the cytoplasm) was observed in 68% of surgically resected NSCLCs (220 of 326) and 82% of SCLCs (14 of 17), whereas no staining was observed in any of normal lung tissues examined (Fig. 1*C*). Positive staining was also observed in all of three large cell neuroendocrine carcinomas. The positive signal by anti-NMU antibody obtained in lung cancer tissues was completely diminished by preincubation of the antibody with recombinant human NMU, indicating its high specificity to NMU protein (Supplementary Fig. S1*C*). We found that patients with NSCLC with NMU-positive tumors showed shorter survival times than patients whose tumors were negative for NMU (P = 0.0363 by the log-rank test; Fig. 1*D*). By univariate analysis, pT (T_1 versus T_{2-4}), pN (N_0 versus N_{1-2}), age (<65 versus ≥65), gender (female versus male), and NMU expression (negative versus positive) were all significantly related to poor survival among patients with NSCLC (P = 0.0012, < 0.0001, 0.0024, 0.0237, and 0.0379, respectively). In multivariate analysis of the prognostic factors, only pT stage, pN stage, gender, and age were indicated to be an independent prognostic factor (P = 0.0011, < 0.0001, 0.0495, and 0.0007, respectively), whereas NMU expression could not be an independent factor (P = 0.0909), thus suggesting the relevance of NMU expression in tumor cells to these clinicopathologic factors.

Effect of NMU on the growth of NSCLC cells. To assess whether NMU is essential for the growth or survival of lung cancer cells, we

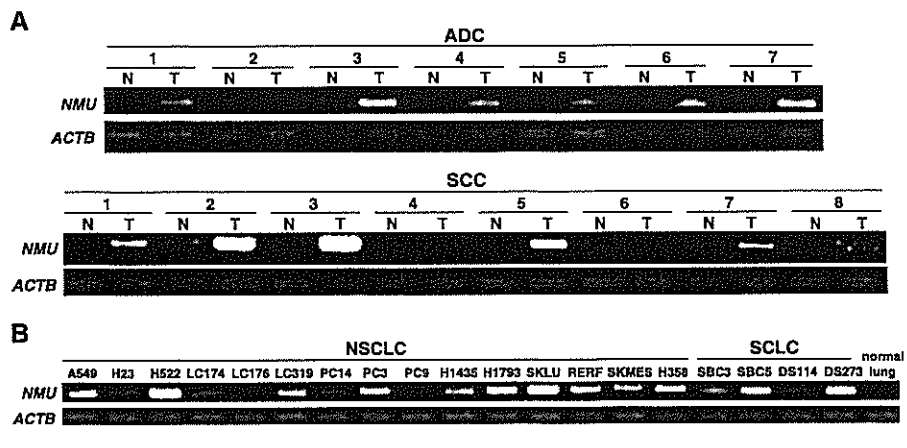

Figure 1. NMU expression in primary lung cancers and cell lines. *A*, expression of *NMU* in clinical samples of NSCLC (*T*) and corresponding normal lung tissues (*N*), examined by semiquantitative RT-PCR. *B*, expression of *NMU* in lung cancer cell lines. *C*, immunohistochemical staining of representative surgically resected and autopsy samples including NSCLC [lung adenocarcinoma (ADC) and squamous cell carcinoma (SCC)] and SCLC as well as normal lung, using anti-NMU antibody on tissue microarrays (original magnification, ×200). *D*, Kaplan-Meier analysis of tumor-specific survival in patients with NSCLC according to NMU expression (P = 0.0363 by the log-rank test).

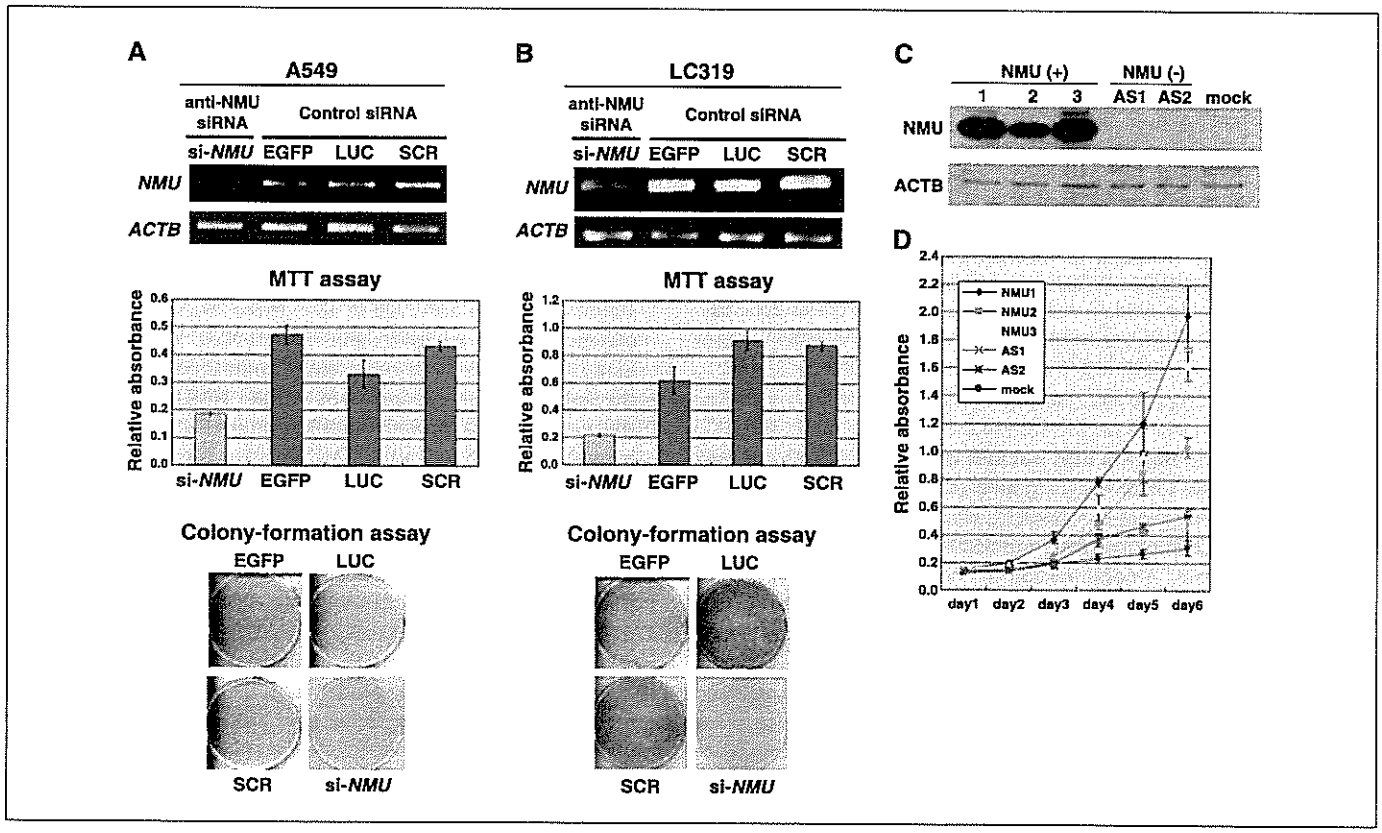

Figure 2. Growth effect of NMU. *A* and *B*, expression of *NMU* in response to si-*NMU* or control siRNAs (EGFP, LUC, or SCR) in A549 (*A*) and LC319 (*B*) cells, analyzed by semiquantitative RT-PCR (*A* and *B*, *top*). Viability of A549 or LC319 cells evaluated by MTT assay in response to si-NMU, -EGFP, -LUC, or -SCR (*A* and *B*, *middle*). Colony formation assays of A549 and LC319 cells transfected with specific siRNAs or control plasmids (*A* and *B*, *bottom*). All experiments were done in triplicate. *C* and *D*, effect of NMU on the growth of COS-7 cells. Expression of NMU in stable transfectants of COS-7 cells on Western blots (*C*). Three independent transfectants expressing high levels of NMU (COS-7-NMU-1, -2, and -3) and controls (COS-7-AS1, -AS2, and mock) were each cultured in triplicate; at each time point, the cell viability was evaluated by the MTT assay (*D*).

designed and constructed plasmids to express siRNA against *NMU* (si-*NMU*), and three different control plasmids [siRNAs for EGFP, Luciferase (LUC), or Scramble (SCR)], and transfected them into A549 (Fig. 2*A*) and LC319 (Fig. 2*B*) cells to suppress the expression of endogenous *NMU*. The amount of *NMU* transcript in the cells transfected with si-*NMU* was significantly decreased in comparison with cells transfected with any of the three control siRNAs (Fig. 2*A* and *B*, *top*); transfection of si-*NMU* also resulted in significant decreases in cell viability and colony numbers measured by MTT and colony formation assays (Fig. 2*A* and *B*, *middle* and *bottom*).

Autocrine growth-promoting effect of NMU. To disclose the potential role of NMU in tumorigenesis, we prepared plasmids designed to express either *NMU* (pcDNA3.1-*NMU*-myc/His) or a complementary strand of *NMU* (pcDNA3.1-antisense). We transfected each of these two plasmids into COS-7 cells and confirmed the expression of NMU protein in cytoplasm and Golgi structures by immunocytochemical staining using anti-NMU antibody (data not shown).

To determine the effect of NMU on the growth of mammalian cells, we carried out a colony formation assay of COS-7-derived transfectants that stably expressed NMU. Immunocytochemical analysis using anti-NMU antibody detected NMU protein in >90% of the COS-7 cells in the culture (Supplementary Fig. S2*A*). We established three independent COS-7 cell lines expressing exogenous NMU (COS-7-NMU-1, -2, and -3; Fig. 2*C*), and compared their growth with control cells transfected with antisense strand or mock vector (COS-7-AS-1 and -2; COS-7-mock). Growth of all of the three COS-7-NMU cells was promoted at a significant degree in accordance with the expression level of NMU (Fig. 2*D*). There was also a remarkable tendency in COS-7-NMU cells to form larger colonies than the control cells (Supplementary Fig. S2*B*). Furthermore, we did colony formation assays to investigate whether the NMU could act as a growth-promoting factor for lung-cancer cells (LC319). The number of geneticin-resistant colonies was significantly increased in dishes containing LC319 cells that had been transfected with the sense strand of cDNA (pcDNA3.1-*NMU*-myc/His) corresponding to the normal transcript, in comparison to cells transfected with the mock vector (Supplementary Fig. S2*C*).

As the immunohistochemical analysis on tissue microarray had indicated that lung cancer patients with NMU-positive tumors showed shorter cancer-specific survival periods than patients whose tumors were negative for NMU, we did Matrigel invasion assays using COS-7-NMU cells. Invasion of COS-7-NMU cells through Matrigel was significantly enhanced, compared with the control cells transfected with mock plasmids, suggesting that NMU could also contribute to the highly malignant phenotype of lung cancer cells (Supplementary Fig. S2*D*).

Subsequently, we carried out autocrine assays using the active form of a 25–amino acid polypeptide of commercially available NMU (NMU-25). To investigate whether NMU-25 would affect cell growth, we incubated COS-7 cells with either NMU-25 or BSA (control) at final concentrations of 0.3 to 15 μmol/L in the culture medium. COS-7 cells incubated with NMU-25 showed enhancement of the cell

growth by MTT and colony formation assays, compared with the control, in a dose-dependent manner (Fig. 3*A* and *B*). We also detected by flow cytometry that rhodamine-labeled NMU-25 peptide bound to the surface of COS-7 cells in a dose-dependent manner (Fig. 3*C*). The results suggested that the growth-promoting effect of NMU was likely to be mediated through binding of NMU-25 to a receptor(s) on the cell surface of COS-7. Subsequently, we investigated whether anti-NMU antibody (0.5-7.5 μmol/L) could inhibit the growth of COS-7 cells cultured in medium containing 3 μmol/L of NMU-25. Expectedly, growth enhancement caused by the addition of 3 μmol/L of NMU-25 was neutralized by the 7.5 μmol/L concentration of anti-NMU antibody, and the viability of COS-7 cells became almost equivalent to that of cells cultured without NMU-25 (Fig. 3*D*).

We then investigated the effect of anti-NMU antibody (0.5-7.5 μmol/L) on the growth of two lung cancer cell lines, LC319 and A549, which showed high levels of endogenous *NMU* expression. The growth of both lines were suppressed by the addition of anti-NMU antibody into their culture media, in a dose-dependent manner ($P < 0.0001$, $P = 0.0002$, respectively; each paired t test), whereas that of LC176 cells expressing NMU at a hardly detectable level was not affected (Supplementary Fig. S3). These data indicated that NMU functions as an autocrine/paracrine growth factor for the proliferation of NSCLC cells.

GHSR1b/NTSR1 as receptors for NMU in a growth-promoting pathway. Two known NMU receptors, NMU1R (FM3/GPR66) and NMU2R (FM4), play important roles in energy homeostasis (17–19). NMU1R is present in many peripheral human tissues (17–19), but NMU2R is only located in the brain. To investigate whether *NMU1R* and *NMU2R* genes were expressed in NSCLCs and whether it is responsible for the growth-promoting effect, we analyzed the expression of these NMU receptors in normal human brain and lung, in NSCLC cell lines, and in clinical tissues by semiquantitative RT-PCR experiments. Neither *NMU1R* nor *NMU2R* expression was detected in any of the lung cancer cell lines or clinical cancer samples examined, although *NMU1R* was expressed in the lung and *NMU2R* in the brain (data not shown), suggesting that NMU is likely to mediate its growth-promoting effect through interaction with other receptor(s) in lung cancer cells.

NMU1R and NMU2R were originally isolated as homologues of known neuropeptide GPCRs. We speculated that unidentified NMU receptor(s) having some degree of homology to NMU1R/NMU2R would be involved in the signaling pathway and searched for candidate NMU receptors using the BLAST program. The homology and expression patterns of genes in NSCLCs in our expression profile data picked up GHSR1b and NTSR1 as good candidates. GHSR has two transcripts, types 1a and 1b. The human GHSR type 1a cDNA encodes a predicted polypeptide of 366 amino acids with seven transmembrane domains, a typical feature of G protein–coupled receptors. A single intron separates its open reading frame into two exons encoding transmembrane domains 1 to 5 and 6 to 7, placing GHSR1a into the intron-containing class of GPCRs. Type 1b is a nonspliced mRNA variant transcribed from a single exon that encodes a polypeptide of 289 amino acids with five transmembrane domains. Our semiquantitative RT-PCR analysis using specific primers for each variant indicated that *GHSR1a* was not expressed in NSCLCs. On the other hand, *GHSR1b* and *NTSR1* were expressed at a relatively high level in some NSCLC cell lines, but not in normal lung (Fig. 4*A*). The *GHSR1b* product reveals 46% homology to NMU1R, and *NTSR1* encodes 418 amino acids with 47% homology to NMU1R. COS-7 cells examined using the autocrine growth-promoting effect of NMU as described above, were confirmed by semiquantitative RT-PCR analysis to endogenously express both *GHSR1b* and *NTSR1* (data not shown). Furthermore, we did immunohistochemical analysis with anti-GHSR1b and anti-NTSR1 polyclonal antibodies using tissue microarrays consisting of 326 NSCLC tissues. Of the 326 cases, GHSR1b staining was positive for 218 (67%; Fig. 4*B, top*), and 217 cases were positive for NTSR1 (67%; Fig. 4*B, bottom*). The expression pattern of GHSR1b or NTSR1 was significantly concordant with NMU expression in these tumors ($\chi^2 = 68$ and 79; $P < 0.0001$ and <0.0001, respectively).

To investigate the binding of NMU-25 to the endogenous GHSR1b and NTSR1 on the NSCLC cells, we did receptor-ligand binding assay using LC319 and PC14 cells treated with NMU-25 (1 μmol/L). We detected binding of Cy5-labeled NMU-25 to the surface of these two cell lines that had endogenously expressed both novel candidate receptors (GHSR1b and NTSR1), but expressed no detectable NMU1R/NMU2R (Fig. 4*A*). The binding activity was elevated in a dose-dependent manner (data not

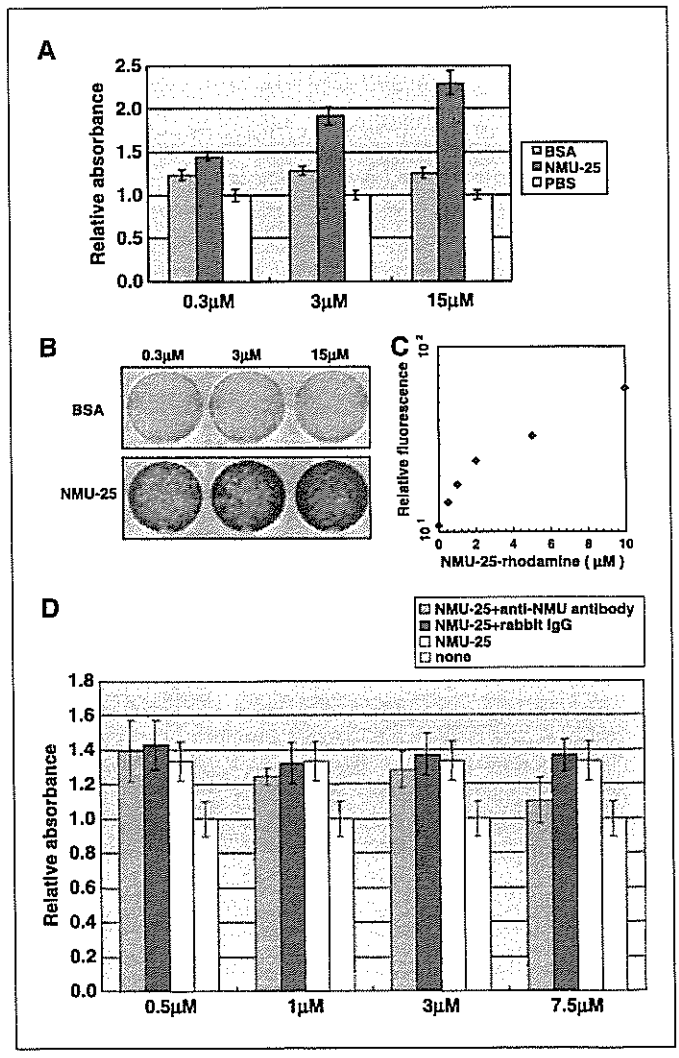

Figure 3. Autocrine effect of NMU on growth of mammalian cells. *A* and *B*, cell viability (*A*) and numbers (*B*) counted by MTT and colony formation assays (COS-7 cells treated with NMU-25 in final concentrations of 0.3-15 μmol/L). *C*, flow cytometric analysis detecting the levels of rhodamine-labeled NMU-25 peptide bound to the surface of COS-7 cells (0-10 μmol/L; *y* axis). *D*, MTT assay evaluating the competitive-binding effect of anti-NMU antibody (0.5-7.5 μmol/L; *y* axis) on the activity of NMU-25 peptide (3 μmol/L) in the culture medium of COS-7 cells.

shown) and was inhibited by the addition of a 10-fold excess of unlabeled NMU-25 as a competitor (Fig. 4*C*, *top* and *bottom*), suggesting the specific interaction of NMU-25 to these cells.

Biologically active ligands for GPCRs have been reported to bind specifically to their cognate receptors and cause an increase in second messengers such as intracellular-Ca^{2+} and/or cAMP levels. We therefore determined the ability of NMU for the induction of these second messengers in LC319 cells through its interaction with GHSR1b/NTSR1. Enhancement of cAMP production (Fig. 4*D*), but not of Ca^{2+} flux, was detected by NMU-25 in a dose-dependent manner in LC319 cells that expressed both GHSR1b and NTSR1, when the cells were cultured in the presence of NMU-25 in final concentrations of 3 to 100 μmol/L in the culture media (data not shown). The results showed that NMU-25 activated the NMU-25-related signaling pathway possibly through functional GHSR1b/NTSR1 in NSCLC cells. This effect was likely to be NMU-25-specific, because the addition of the same amount of GHRL and NTS, known ligands for GHSR/NTSR1, did not enhance cAMP production (Fig. 4*D*). On the other hand, treatment with NTS, but not that with GHRL, caused the mobilization response of intracellular Ca^{2+} in LC319 cells (data not shown), similar to previous reports (23, 24), suggesting the ligand-dependent and diverse physiologic function of GHSR1b and/or NTSR1 in mammalian cells.

We then examined the biological significance of the NMU-receptor interaction in pulmonary carcinogenesis using plasmids designed to express siRNA against *GHSR* or *NTSR1* (si-*GHSR-1*, si-*NTSR1-1*, and si-*NTSR1-2*). Transfection of either of these plasmids into LC319 or A549 cells suppressed the expression of the endogenous receptor in comparison with cells containing any of the three control siRNAs (Supplementary Fig. S4, *top*). In accordance with the reduced expression of the receptors, LC319 and A549 cells showed significant decreases in cell viability and number of colonies (Supplementary Fig. S4, *middle* and *bottom*). These results strongly support the possibility that NMU, by interaction with GHSR1b and NTSR1, might play a very significant role in the development/progression of lung cancer.

Internalization of GHSR1b/NTSR1 receptors after binding with NMU. To determine the mechanism involved in the regulation

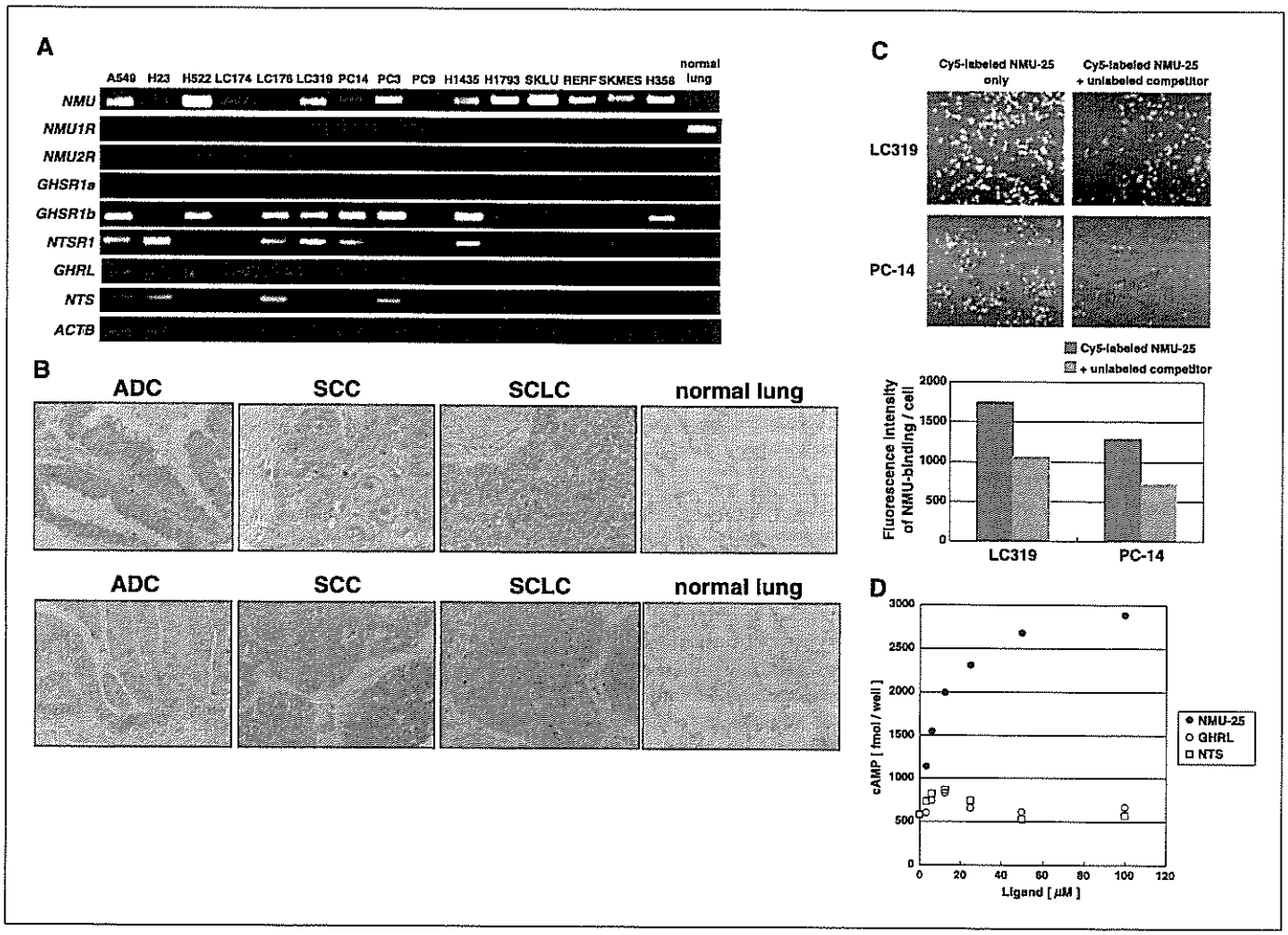

Figure 4. Functional association of NMU with endogenous GHSR1b/NTSR1 on the NSCLC cells. *A*, expression of *NMU*, candidate receptors, and their known ligands as detected by semiquantitative RT-PCR analysis in NSCLC cell lines. *B*, immunohistochemical staining of representative surgically resected and autopsy samples including NSCLC [lung adenocarcinoma (ADC) and squamous cell carcinoma (SCC)] and SCLC as well as normal lung, using anti-NTSR1 (*top*) or anti-GHSR1b (*bottom*) antibody (original magnification, ×200). *C*, binding of Cy5-labeled NMU-25 to the cell surface of NSCLC cells analyzed by laser scanning imaging. Digital fluorescence images of Cy5-labeled NMU-25 (1 μmol/L) bound to LC319 and PC14 cells with/without 10 μmol/L of nonlabeled NMU-25 peptides as a competitor was detected by the 8200 Cellular Detection System (*top*). *Columns*, the average fluorescence values of Cy5-labeled NMU-25 bound to each cell in duplicate assays (*bottom*). *D*, specific signal transduction by NMU as represented by cAMP release in LC319 cells. Dose-response curves of intracellular cAMP production by NMU-25 (●), GHRL (○), or NTS (□) treatment (3-100 μmol/L) in LC319 cells were shown.

of NMU-GHSR1b/NTSR1 signaling, we examined whether GHSR1b/NTSR1 is internalized when they are exposed to NMU, through confocal microscopy observation of the subcellular distribution of the two receptors after NMU-25 stimulation. After they were introduced in COS-7 cells, the GHSR1b and NTSR1 receptors were mainly colocated at the plasma membrane in the condition without the exposure to NMU-25. However, once NMU-25 was added to the cell culture, both of the receptors were cointernalized and predominantly formed the vesicle-like structures in a time-dependent manner (Fig. 5*A*). Similarly, in LC319 cells, in which GHSR1b and NTSR1 were endogenously overexpressed, NMU stimulation induced the cointernalization of the two receptors (Supplementary Fig. S5). The results suggest the possible physical interaction between GHSR1b and NTSR1, as well as NMU-induced cointernalization.

To further confirm whether NMU is internalized after binding to its receptors, internalization of NMU was investigated using Alexa Fluor 594–labeled NMU-25 (NMU-25-Alexa 594) and a confocal microscopy. The binding of agonists to GPCRs on the cell surface is generally known to initiate receptor-mediated endocytosis. In the course of this process, receptors are passed through multiple intracellular pathways that lead to lysosomal degradation or recycling them to the cell surface (25, 26). On the other hand, far less is known about whether all GPCR ligands are internalized together with their receptor. In the case of neuropeptides, the ligand is usually internalized with its receptor (27, 28). As shown in Fig. 5*B*, the *xz*- and *yz*-projections indicated that NMU-25-Alexa 594 was incorporated within the cells. After 15 minutes of incubation, the internalized ligand was concentrated in dots or irregular clusters at more peripheral parts of the cytoplasm in cells (Fig. 5*B*, *left*). In contrast, after 45 minutes of incubation, fluorescence was concentrated within small spots clustered in the center of the cells, close to the nucleus (Fig. 5*B*, *right*). These results are similar to the previous reports demonstrating that internalization of NTS proceeded through small endosome-like organelles and the internalized ligand to accumulate at the core of the cell surrounding the nucleus (29).

Functional receptor dimerization of GHSR1b and NTSR1. To examine the direct association between GHSR1b and NTSR1, we transiently expressed either FLAG-tagged GHSR1b or FLAG-tagged NTSR1 individually, and also coexpressed both the FLAG-tagged receptors in COS-7 cells (representative data for GHSR1b was shown in Fig. 5*C*). COS-7 cells were confirmed by semiquantitative RT-PCR analysis to endogenously express both *GHSR1b* and *NTSR1*, but not NMU. Cell lysates preincubated with the cross-linking reagent were immunoprecipitated by anti-FLAG antibody, and were served for Western blot analysis using anti-FLAG, anti-NTSR1, or anti-GHSR antibody. We found coprecipitation of the following proteins: the GHSR1b monomer (~30 kDa), the NTSR1 monomer (~45 kDa), the GHSR1b/NTSR1 heterodimer (~70-75 kDa), the GHSR1b homodimer (~60-65 kDa), and the NTSR1 homodimer (~90-95 kDa; Fig. 5*C*). No such species were detected when empty vector (mock) was transfected to COS-7 cells as a negative control. In the cells expressing only FLAG-tagged NTSR1 and those coexpressing both the FLAG-tagged receptors (NTSR1 and GHSR1b), similar results were observed (data not shown). These results confirm an interaction between GHSR1b and NTSR1, implying the existence of a GHSR1b/NTSR1 heterodimer.

To further confirm the functional importance of the activation and heterodimerization of GHSR1b and NTSR1 at the signal transduction level, we examined the dose-dependent intracellular cAMP production by NMU-25 in lung cancer cell lines representing various expression patterns of the two receptors as detected by semiquantitative RT-PCR analysis (Fig. 5*D*). In LC319 cells expressing high levels of both receptors, treatment with NMU-25 resulted in a marked and reproducible cAMP accumulation (Fig. 5*D*, *top left*). RERF-LC-AI cells expressing low levels of both receptors, showed significant but low cAMP production in response to NMU-25 (Fig. 5*D*, *top right*). NCI-H358 and SK-MES-1 cells expressing either of the receptors did not show detectable cAMP production (Fig. 5*D*, *bottom*).

Identification of downstream genes of NMU. To further elucidate the NMU-signaling pathway, siRNA against *NMU* (si-*NMU*) or LUC (control siRNA) were transfected into LC319 cells overexpressing *NMU*, and genes that were down-regulated in the former cells were screened using a cDNA microarray containing 32,256 genes. By this approach, we selected 70 genes whose expression was significantly decreased in accordance with *NMU* suppression by performing the self-organizing map clustering analysis (22). Semiquantitative RT-PCR analysis confirmed the reduction of candidate transcripts in a time-dependent manner in LC319 cells transfected with si-*NMU*, but not with control siRNA for LUC (Fig. 6*A*). We also evaluated the transactivation of these genes in accordance with the introduction of *NMU* expression in lung cancer cell lines (data not shown) and finally identified six candidate NMU-target genes, *FOXM1, GCDH, CDK5RAP1, LOC134145, NUP188*, and one unannotated transcript (clone IMAGE: 3839141; Fig. 6*B*). Among these six genes selected, *FOXM1* mRNA levels were found to be significantly elevated in clinical cases of lung cancer and showed good concordance with expression levels of *NMU* and two receptors, *GHSR1b* and *NTSR1* (Fig. 6*C*). To validate the induction of the *FOXM1* expression by the NMU ligand-receptor signaling, we cultured LC319 cells expressing GHSR1b and NTSR1 in the presence of NMU-25 or BSA (control) at final concentrations of 25 μmol/L in the culture media, and confirmed an enhanced expression of *FOXM1* in the NMU-treated cells (Fig. 6*D*). Furthermore, we did immunohistochemical analysis of NSCLCs with anti-FOXM1 polyclonal antibodies using tissue microarrays. Of the 325 cases of NSCLC available for this assay, FOXM1 staining was positive for 230 (70.8%; Supplementary Fig. S6*A*). The expression pattern of FOXM1 was significantly concordant with NMU expression in these tumors ($\chi^2 = 68$; $P < 0.0001$). We found that patients with NSCLC with FOXM1-positive tumors showed shorter survival times than patients whose tumors were negative for FOXM1 ($P = 0.0495$ by the log-rank test; Supplementary Fig. S6*B*). These results independently show that NMU, by the interaction with GHSR1b/NTSR1 heterodimer and subsequent activation of its downstream targets, such as *FOXM1*, could significantly affect the growth and malignant nature of lung cancer cells.

Discussion

Recent acceleration in the identification and characterization of novel molecular targets for cancer therapy has stimulated considerable interest in the development of new types of anticancer agents (3). Molecular-targeted drugs are expected to be highly specific to malignant cells, with minimal risk of adverse effects due to their well-defined mechanisms of action. As a promising strategy to identify such molecules, we combined the power of genome-wide expression analysis with high-throughput screening of loss-of-function effects by means of the RNAi technique. In addition, we used tissue microarrays to analyze hundreds of archived clinical samples for validation of the potential target proteins. Using this approach, we have shown here that *NMU* and its cancer-specific receptors, as well as its target genes,

are frequently overexpressed in clinical samples of lung cancer and in cell lines, and that those gene products play indispensable roles in the growth and progression of lung cancer cells.

A COOH-terminal asparaginamide structure and the COOH-terminal heptapeptide core of NMU protein are essential for its contractile activity in smooth muscle cells (30). Recent studies have indicated that NMU acts at the hypothalamic level to inhibit food intake; therefore, this protein might be a physiologic regulator of feeding and body weight (18, 31, 32). NMU was also expressed in several types of human tumors (33–35), but no reports have thus far suggested the involvement of NMU overexpression in pulmonary carcinogenesis, and its precise biological function in cancer cells have never been clarified.

Our treatment of NSCLC cells with specific siRNA to reduce the expression of *NMU* resulted in growth suppression. We also found other evidence supporting the significance of this pathway in carcinogenesis; e.g., the addition of NMU into the medium promoted the growth of COS-7 cells in a dose-dependent manner. The expression of NMU also resulted in the significant promotion of cell growth and invasion in *in vitro* assays. Moreover, clinicopathologic evidence obtained through our tissue microarray experiments showed that NSCLC patients with tumors expressing NMU showed shorter cancer-specific survival periods than those with negative NMU expression. The results obtained by *in vitro* and *in vivo* assays strongly suggested that overexpressed NMU is likely to be an important growth factor and might be associated with cancer cell growth and invasion, functioning in an autocrine manner, and that screening molecules targeting the NMU receptor growth-promoting pathway should be a promising therapeutic approach for treating lung cancers. Because NMU is a secreted protein and most of the clinical NSCLC samples used for our analysis were at an early and operable stage, NMU might also serve as a biomarker for diagnosis of early stage lung cancer, as well as an indicator for a highly malignant phenotype of lung cancer cells, in combination with fiberscopic transbronchial biopsy or blood tests.

NMU was already known to interact with at least two receptors, NMU1R (FM3/GPR66) and NMU2R (FM4), each of which has seven predicted α-helical transmembrane domains containing highly conserved motifs, as do other members of the rhodopsin GPCR family (17–19). The results presented here, however, indicated that these two known receptors were not the targets for the autocrine NMU-signaling pathway in NSCLCs; instead, the *GHSR1b* and

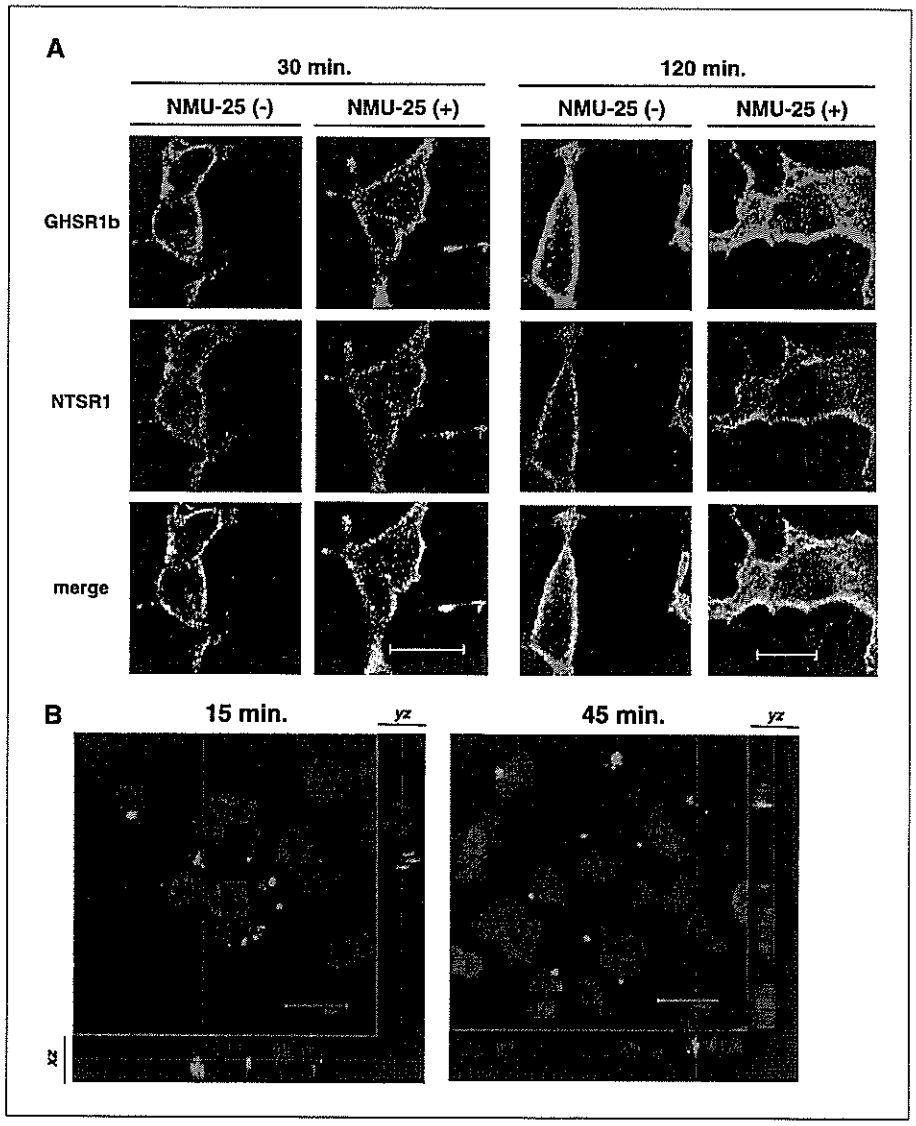

Figure 5. Characterization of GHSR1b/NTSR1 heterodimers and their internalization as cognate receptors for NMU. *A*, internalization of GHSR1b/NTSR1 protein induced by NMU-25. COS-7 cells transiently expressing both GHSR1b and NTSR1 were exposed to NMU-25 (10 μmol/L) for 30 minutes (*left*) or 120 minutes (*right*). COS-7 cells without exposure to the NMU-25 treatment served as controls. Cells were subsequently fixed and stained using secondary antibodies conjugated to Alexa Fluor 488–labeled anti-GHSR antibody or Alexa Fluor 594–labeled anti-NTSR1 antibody. Subcellular distribution of the two receptor proteins was examined by confocal microscopy. *Bottom*, LC319 cells expressing both endogenous GHSR1b and NTSR1 were exposed to NMU-25 (10 μmol/L) for 30 minutes (*left*) or 120 minutes (*right*). *B*, internalization of NMU-25-Alexa 594 in LC319 cells. The cells were incubated with 35 μmol/L of NMU-25-Alexa 594 for 15 minutes (*left*) or 45 minutes (*right*) at 37°C, and subsequently washed and fixed. *Red*, NMU-25-Alexa 594; *blue*, cell nuclei (with DAPI). The *xz*- and *yz*-projections proved that the ligands were localized within the cells. *Dotted lines*, where the *xz*- and *yz*-projections were taken.

NTSR1 heterodimer was implied to be the possible targets for the growth-promoting effect of NMU in lung tumors. GHSR is a known receptor of GHRL, a recently identified 28–amino acid peptide capable of stimulating the release of pituitary growth hormone and appetite in humans (23, 36, 37). Of the two transcripts known to be receptors for GHRL, GHSR1a and GHSR1b, we detected overexpression of only *GHSR1b* in NSCLC tissues and cell lines. In NSCLC, GHRL was not significantly expressed in the cell lines examined (Fig. 4*A*), therefore, we suspected that GHSR1b could have a growth-promoting function in lung tumors through binding to NMU, but not to GHRL. Interestingly, it was reported that *GHRL* and *GHSR1b*, but not *GHSR1a* genes were overexpressed in the erythroleukemic HEL cells, whose proliferation was regulated by des-acyl GHRL in an autocrine manner (38). NTSR1 is one of three receptors of NTS, a brain and gastrointestinal peptide that fulfills many central and peripheral functions (24). NTS modulates the transmission of dopamine and secretion of pituitary hormones, and exerts hypothermic and analgesic effects in the brain, whereas it functions as a peripheral hormone in the digestive tract and cardiovascular system. Others have reported that NTS is produced and secreted in several human cancers, including SCLCs (24). We detected the expression of *NTS* in 4 of the 15 NSCLC cell lines we

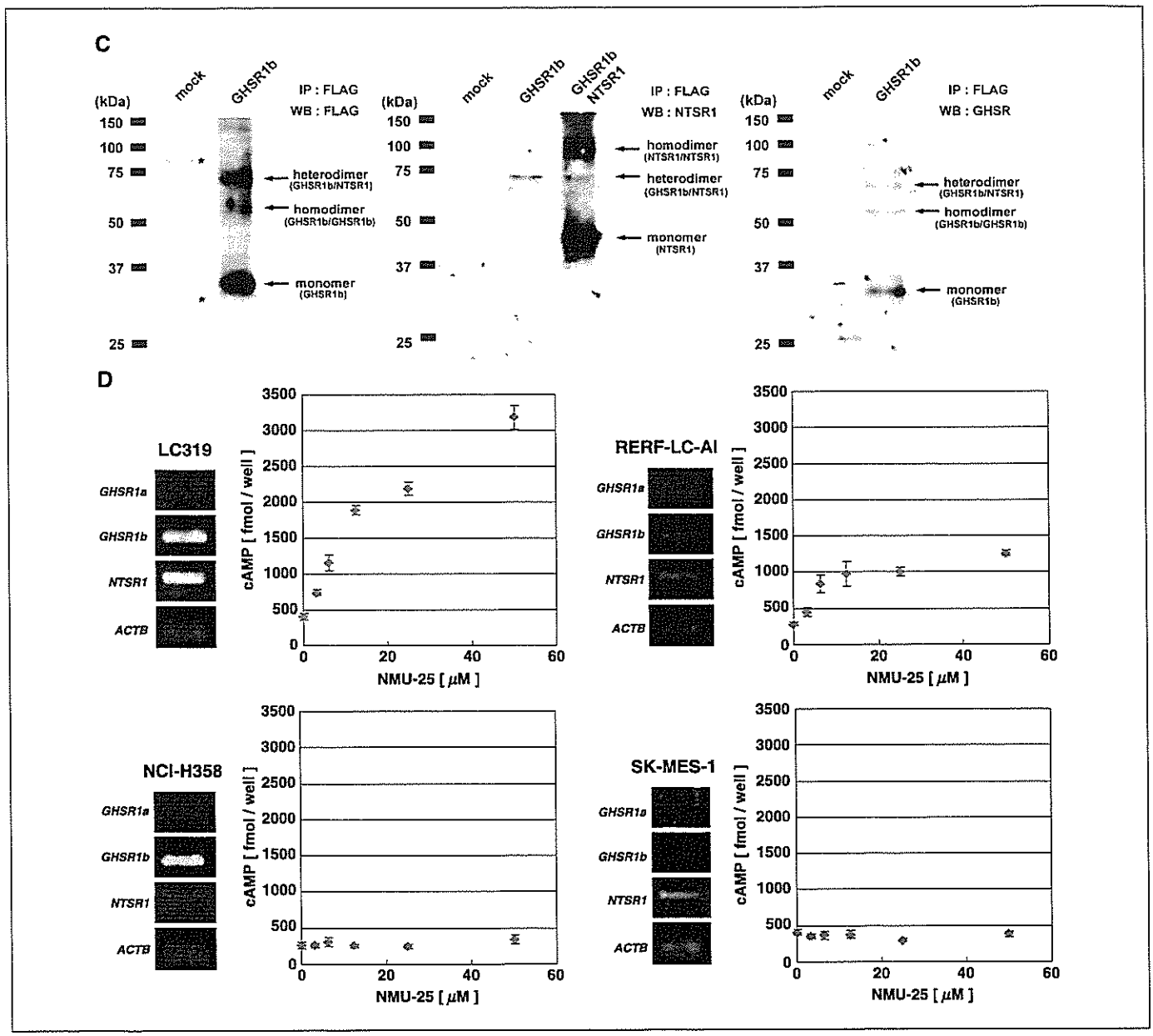

Figure 5 *Continued. C,* immunoprecipitation of cell lysates from COS-7 cells transiently expressed FLAG-tagged GHSR1b, and ones coexpressed both FLAG-tagged GHSR1b and NTSR1. The proteins immunoprecipitated by anti-FLAG antibody were subjected to SDS-PAGE and immunoblotted with anti-FLAG antibody (*left*), with anti-NTSR1 antibody (*middle*), or with anti-GHSR antibody (*right*). *Arrows,* monomers, heterodimers, and homodimers of the receptors. The molecular weight (kDa) markers are indicated on the left side of individual panels; *, nonspecific immunoreactive protein band detected by anti-FLAG antibody. *D,* relationship between the expression levels of GHSR1b/NTSR1 and intracellular cAMP production by NMU-25 in lung cancer cell lines. The expression levels of receptors in LC319, RERF-LC-AI, NCI-H358, and SK-MES-1 cells were detected by semiquantitative RT-PCR analysis. Dose-response curves of intracellular cAMP production by NMU-25 treatment (3-50 μmol/L) in individual cell lines are shown. All experiments were done in triplicate.

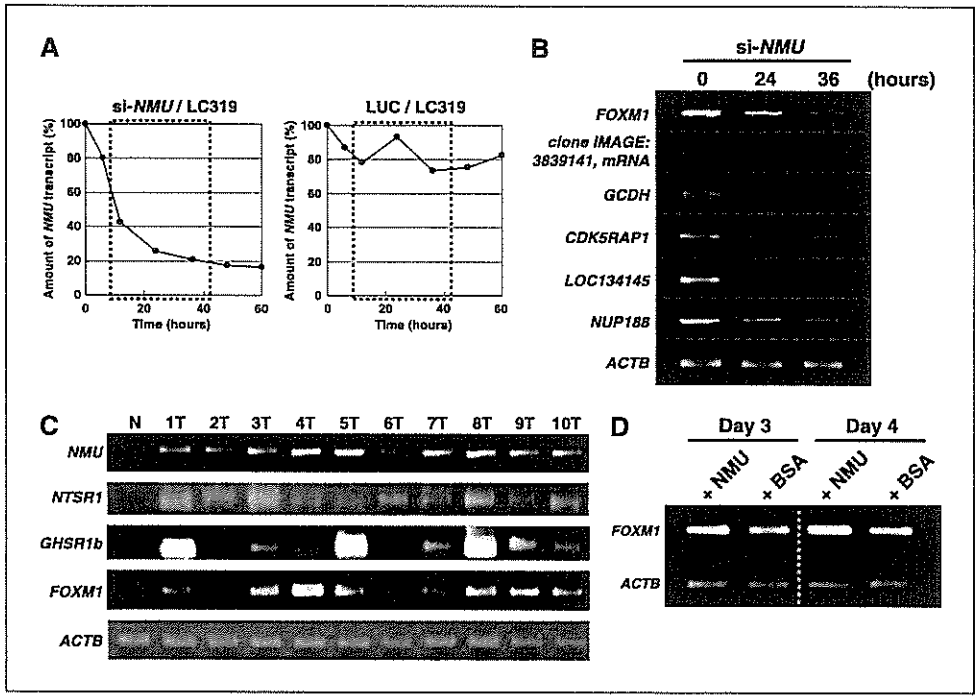

Figure 6. Identification of candidate downstream genes of the NMU signaling. *A*, time-dependent reduction of the *NMU* gene expression monitored by semiquantitative RT-PCR experiments of the mRNAs from LC319 cells treated with si-*NMU*, using *NMU*-specific primers. We prepared appropriate dilutions of each single-stranded cDNA prepared from mRNAs of LC319 cells at several time points. The β-actin (*ACTB*) expression was used as a quantitative control. Densitometric intensity of PCR product was quantified by image analysis software (Quantity One; Bio-Rad, Hercules, CA). *B*, time-dependent reduction of expression levels for possible target genes in the NMU signaling pathway was confirmed by semiquantitative RT-PCR experiments of mRNAs prepared from LC319 cells that were treated with si-*NMU*. Individual gene-specific primers were used for PCR amplification. *C*, expression of *NMU*, *NTSR1*, *GHSR1b*, and *FOXM1* in clinical NSCLC samples (*T*, lung tumor; *N*, normal lung tissue), examined by semiquantitative RT-PCR. *D*, induction of *FOXM1* expression in LC319 cells incubated with NMU-25, detected by semiquantitative RT-PCR using mRNAs prepared from LC319 cells treated with NMU-25 or BSA (as control; 25 μmol/L).

examined (Fig. 4*A*), but the expression pattern of *NTS* was not necessarily concordant with that of *NMU* or *NTSR1*. Therefore, we assume that NTS might contribute to the growth of NSCLC through NTSR1 or other receptor(s) in a small subset of NSCLCs.

In our experiments, the majority of the cancer cell lines and clinical NSCLCs that expressed NMU also expressed GHSR1b and NTSR1, indicating that these ligand-receptor interactions were likely to be involved in a pathway that is central to the growth-promoting activity of NMU in NSCLCs. *GHSR* and *NTSR1* were also expressed in COS-7 cells used to examine the growth and invasion effect of NMU; the data strongly supported the importance of these two receptors for oncogenesis. Our experiments further revealed that NMU-25 functionally bound to these receptors on the cell surface of NSCLC cells and subsequently induced the production of a second messenger, cAMP. We also showed that treatment of NSCLC cells with siRNAs for *GHSR* or *NTSR1* reduced the expression of these receptors and resulted in cancer growth inhibition. Elevated cAMP levels were generally observed via activation of adenylate cyclase, which activated protein kinase A (PKA). It was reported that GHRL did not displace ^{125}I-labeled rat NMU binding to NMU1R-expressing cells when tested at concentrations up to 10 mmol/L (39). However, GHRL or NTS competitively inhibited NMU-induced cAMP production in NSCLC cells.[8] Moreover, we provide biochemical and physiologic evidence for the internalization and heterodimerization of the two neuropeptide GPCRs, GHSR1b and NTSR1 (Fig. 5*A*; Supplementary Fig. S5). These results independently suggest that NMU stimulates NSCLC cell proliferation by a pathway through the GHSR1b-NTSR1 heterodimer whose function is quite different from the two known NMU-receptors, NMU1R and NMU2R. Heterodimerization has been shown to contribute to both ligand-binding affinity and signaling efficacy of GPCRs (40, 41). Heterodimers can be formed by receptors for various ligands/transmitters; for example, GPCRs for angiotensin and bradykinin (42), or those for opioid and adrenergic ligands (43). Moreover, it has been reported that coexpression of GHSR1a and GHSR1b resulted in an attenuation of the signaling capability of GHSR1a, suggesting that GHSR1b possibly interacted with GHSR1a through receptor heterodimerization (44). Based on the fact that GHSR1b exhibits no function towards GHRL (45), heterodimerization of GHSR1a and GHSR1b might in fact be a common feature for GHSR. The combination of our data with previous reports suggests that binding of NMU to GHSR1b/NTSR1 heterodimer, which cooperated with G proteins of the G_s subfamily, leads to the activation of adenylate cyclase, accumulation of intracellular cAMP, and activation of cAMP-dependent protein kinase (PKA), and that the subsequent release of catalytic subunits of PKA (C) from the regulatory subunits (R) activates downstream target genes, thus, finally resulting in the activation of growth-promoting pathways.

Microarray data of LC319 cells treated with siRNA for *NMU* suggests that the NMU signaling pathway could affect the growth promotion of lung cancer cells by transactivating a set of downstream genes. We provided evidence that the FOXM1 transcription factor is one of the downstream targets in the NMU signaling pathway. In our tissue microarray experiments, we observed that the expression pattern of FOXM1 was significantly concordant with that of NMU in the same set of tumors, and that lung cancer patients with FOXM1-positive tumors showed shorter survival periods than patients with FOXM1-negative tumors, thus, independently confirming the effect of NMU-FOXM1 signaling on the promotion of the malignant nature of lung cancer cells. FOXM1 was known to be overexpressed in several types of human cancers (46–48). We also confirmed that treatment of NSCLC cells with specific siRNA to reduce the expression of *FOXM1* resulted in growth suppression.[8] To predict the transcriptional regulation of the *FOXM1* gene by cAMP-response element (CRE)–binding protein, we also screened the CRE-like sequence within a 1-kb upstream region of the putative transcription start sequence using the computer prediction program and found that the region

[8] Unpublished data.

contains three CRE-like elements (data not shown). Moreover, it should be noted that the luciferase reporter gene assay suggested that two of the CRE-like sequences are essential for effective augmentation of *FOXM1* promoter activity following NMU stimulation.[8] We speculate that CRE-binding proteins phosphorylated by PKA might be directly responsible for the regulation of *FOXM1* expression. Previous reports suggested that some cyclin genes are possible transcription targets of FOXM1 transcription factor and that FOXM1 controls the transcription network of genes which are essential for cell division and exit from mitosis (29). In fact, we observed the activation of *CCNB1* and *CCNA2* in the majority of a series of clinical NSCLC we examined and its good concordance of the expression to *FOXM1* expression. These data indicate the possibility that the NMU-FOXM1 pathway is finally linked to cyclin-dependent pathways.

In summary, we have shown that NMU and the recently identified heterodimerization of GHSR1b and NTSR1 are likely to play an essential role for an autocrine growth-promoting pathway in NSCLCs by modulating the transcription of downstream target genes including *FOXM1*. The data reported here strongly imply the possibility of designing new anticancer drugs, specific for lung cancer, that target the NMU-GHSR1b/NTSR1 pathway as well as the development of novel diagnostic/prognostic markers for lung cancer.

Acknowledgments

Received 4/18/2006; revised 7/24/2006; accepted 8/4/2006.

Grant support: "Research for the Future" Program Grant of The Japan Society for the Promotion of Science (no. 00L01402) to Y. Nakamura.

The costs of publication of this article were defrayed in part by the payment of page charges. This article must therefore be hereby marked *advertisement* in accordance with 18 U.S.C. Section 1734 solely to indicate this fact.

References

1. Greenlee RT, Hill-Harmon MB, Murray T, Thun M. Cancer statistics. CA Cancer J Clin 2001;51:15–36.
2. Sozzi G. Molecular biology of lung cancer. Eur J Cancer 2001;37:63–73.
3. Schiller JH, Harrington D, Belani CP, et al. Comparison of four chemotherapy regimens for advanced non-small-cell lung cancer. N Engl J Med 2001;346:92–8.
4. Kikuchi T, Daigo Y, Katagiri T, et al. Expression profiles of non-small cell lung cancers on cDNA microarrays: identification of genes for prediction of lymph-node metastasis and sensitivity to anti-cancer drugs. Oncogene 2003;22:2192–205.
5. Kakiuchi S, Daigo Y, Ishikawa N, et al. Prediction of sensitivity of advanced non-small cell lung cancers to gefitinib (Iressa, ZD1839). Hum Mol Genet 2004;13:3029–43.
6. Suzuki C, Daigo Y, Kikuchi T, Katagiri T, Nakamura Y. Identification of COX17 as a therapeutic target for non-small cell lung cancer. Cancer Res 2003;63:7038–41.
7. Suzuki C, Daigo Y, Ishikawa N, et al. ANLN plays a critical role in human lung carcinogenesis through activation of RHOA and by involvement in PI3K/AKT pathway. Cancer Res 2005;65:11314–25.
8. Ishikawa N, Daigo Y, Yasui W, et al. ADAM8 as a novel serological and histochemical marker for lung cancer. Clin Cancer Res 2004;10:8363–70.
9. Ishikawa N, Daigo Y, Takano A, et al. Increases of amphiregulin and transforming growth factor-α in serum as predictors of poor response to gefitinib among patients with advanced non-small cell lung cancers. Cancer Res 2005;65:9176–84.
10. Kato T, Daigo Y, Hayama S, et al. A novel human tRNA-dihydrouridine synthase involved in pulmonary carcinogenesis. Cancer Res 2005;65:5638–46.
11. Furukawa C, Daigo Y, Ishikawa N, et al. PKP3 oncogene as prognostic marker and therapeutic target for lung cancer. Cancer Res 2005;65:7102–10.
12. Minamino N, Kangawa K, Matsuo H. Neuromedin U-8 and U-25: novel uterus stimulating and hypertensive peptides identified in porcine spinal cord. Biochem Biophys Res Commun 1985;130:1078–85.
13. Domin J, Ghatei MA, Chohan P, Bloom SR. Characterization of neuromedin U-like immunoreactivity in rat, porcine, guinea-pig and human tissue extracts using a specific radioimmunoassay. Biochem Biophys Res Commun 1986;140:1127–34.
14. Domin J, Yiangou YG, Spokes RA, et al. The distribution, purification, and pharmacological action of an amphibian neuromedin U. J Biol Chem 1989;264:20881–5.
15. Kage R, O'Harte F, Thim L, Conlon JM. Rabbit neuromedin U-25: lack of conservation of a posttranslational processing site. Regul Pept 1991;33:191–8.
16. Austin C, Oka M, Nandha KA, et al. Distribution and developmental pattern of neuromedin U expression in the rat gastrointestinal tract. J Mol Endocrinol 1994;12:257–63.
17. Fujii R, Hosoya M, Fukusumi S, et al. Identification of neuromedin U as the cognate ligand of the orphan G protein-coupled receptor FM-3. J Biol Chem 2000;275:21068–74.
18. Howard AD, Wang R, Pong SS, et al. Identification of receptors for neuromedin U and its role in feeding. Nature 2000;406:70–4.
19. Funes S, Hedrick JA, Yang S, et al. Cloning and characterization of murine neuromedin U receptors. Peptides 2002;23:1607–15.
20. Chin SF, Daigo Y, Huang HE, et al. A simple and reliable pretreatment protocol facilitates fluorescent *in situ* hybridisation on tissue microarrays of paraffin wax embedded tumour samples. Mol Pathol 2003;56:275–9.
21. Callagy G, Cattaneo E, Daigo Y, et al. Molecular classification of breast carcinomas using tissue microarrays. Diagn Mol Pathol 2003;12:27–34.
22. Kohonen T. The self-organizing map. Proc IEEE 1990;78:1464–80.
23. Kojima M, Hosoda H, Date Y, Nakazato M, Matsuo H, Kangawa K. Ghrelin is a growth-hormone-releasing acylated peptide from stomach. Nature 1999;402:656–60.
24. Heasley LE. Autocrine and paracrine signaling through neuropeptide receptors in human cancer. Oncogene 2001;20:1563–9.
25. Bohm SK, Grady EF, Bunnett NW. Regulatory mechanisms that modulate signalling by G-protein-coupled receptors. Biochem J 1997;322:1–18.
26. Koenig JA, Edwardson JM. Endocytosis and recycling of G protein-coupled receptors. Trends Pharmacol Sci 1997;18:276–87.
27. Ghinea N, Vu Hai MT, Groyer-Picard MT, Houllier A, Schoevaert D, Milgrom E. Pathways of internalization of the hCG/LH receptor: immunoelectron microscopic studies in Leydig cells and transfected L-cells. J Cell Biol 1992;118:1347–58.
28. Vandenbulcke F, Nouel D, Vincent JP, Mazella J, Beaudet A. Ligand-induced internalization of neurotensin in transfected COS-7 cells: differential intracellular trafficking of ligand and receptor. J Cell Sci 2000;113:2963–75.
29. Faure MP, Alonso A, Nouel D, et al. Somatodendritic internalization and perinuclear targeting of neurotensin in the mammalian brain. J Neurosci 1995;15:4140–7.
30. Austin C, Nandha KA, Meleagros L, Bloom SR. Cloning and characterization of the cDNA encoding the human neuromedin U precursor: NMU expression in the human gastrointenstinal tract. J Mol Endocrinol 1995;14:157–69.
31. Ivanov TR, Lawrence CB, Stanley PJ, Luckman SM. Evaluation of neuromedin U actions in energy homeostasis and pituitary function. Endocrinology 2002;143:3813–21.
32. Hanada R, Teranishi H, Pearson JT, et al. Neuromedin U has a novel anorexigenic effect independent of the leptin signaling pathway. Nat Med 2004;10:1067–73.
33. Steel JH, Van Noorden S, Ballesta J, et al. Localization of 7B2, neuromedin B, and neuromedin U in specific cell types of rat, mouse, and human pituitary, in rat hypothalamus, and in 30 human pituitary and extrapituitary tumors. Endocrinology 1988;122:270–82.
34. Shetzline SE, Rallapalli R, Dowd KJ, et al. Neuromedin U: a Myb-regulated autocrine growth factor for human myeloid leukemias. Blood 2004;104:1833–40.
35. Euer NI, Kaul S, Deissler H, Mobus VJ, Zeillinger R, Weidle UH. Identification of L1CAM, Jagged2 and Neuromedin U as ovarian cancer-associated antigens. Oncol Rep 2005;13:375–87.
36. Kim K, Arai K, Sanno N, Osamura RY, Teramoto A, Shibasaki T. Ghrelin and growth hormone (GH) secretagogue receptor (GHSR) mRNA expression in human pituitary adenomas. Clin Endocrinol (Oxf) 2001;54:759–68.
37. Lambert PD, Anderson KD, Sleeman MW, et al. Ciliary neurotrophic factor activates leptin-like pathways and reduces body fat, without cachexia or rebound weight gain, even in leptin-resistant obesity. Proc Natl Acad Sci U S A 2001;98:4652–7.
38. De Vriese C, Gregoire F, De Neef P, Robberecht P, Delporte C. Ghrelin is produced by the human erythroleukemic HEL cell line and involved in an autocrine pathway leading to cell proliferation. Endocrinology 2005;146:1514–22.
39. Kojima M, Haruno R, Nakazato M, et al. Purification and identification of neuromedin U as an endogenous ligand for an orphan receptor GPR66 (FM3). Biochem Biophys Res Commun 2000;276:435–8.
40. Bouvier M. Oligomerization of G-protein-coupled transmitter receptors. Nat Rev Neurosci 2001;2:274–86.
41. Devi LA. Heterodimerization of G-protein-coupled receptors: pharmacology, signaling and trafficking. Trends Pharmacol Sci 2001;22:532–7.
42. AbdAlla S, Lother H, Quitterer U. AT1-receptor heterodimers show enhanced G-protein activation and altered receptor sequestration. Nature 2000;407:94–8.
43. Rocheville M, Lange DC, Kumar U, Patel SC, Patel RC, Patel YC. Receptors for dopamine and somatostatin: formation of hetero-oligomers with enhanced functional activity. Science 2000;288:154–7.
44. Chan CB, Cheng CH. Identification and functional characterization of two alternatively spliced growth hormone secretagogue receptor transcripts from the pituitary of black seabream *Acanthopagrus schlegeli*. Mol Cell Endocrinol 2004;214:81–95.
45. Howard AD, Feighner SD, Cully DF, et al. A receptor in pituitary and hypothalamus that functions in growth hormone release. Science 1996;273:974–7.
46. Teh MT, Wong ST, Neill GW, Ghali LR, Philpott MP, Quinn AG. FOXM1 is a downstream target of Gli1 in basal cell carcinomas. Cancer Res 2002;62:4773–80.
47. van den Boom J, Wolter M, Kuick R, et al. Characterization of gene expression profiles associated with glioma progression using oligonucleotide-based microarray analysis and real-time reverse transcription-polymerase chain reaction. Am J Pathol 2003;163:1033–43.
48. Kalinichenko VV, Major ML, Wang X, et al. Foxm1b transcription factor is essential for development of hepatocellular carcinomas and is negatively regulated by the p19ARF tumor suppressor. Genes Dev 2004;18:830–50.

Original Paper

Pathobiology

Pathobiology 2006;73:93–97
DOI: 10.1159/000094493

Received: January 24, 2006
Accepted: April 12, 2006

Nuclear and Mitochondrial DNA Microsatellite Instability in Gastrointestinal Stromal Tumors

K. Kose[a] T. Hiyama[d] S. Tanaka[c] M. Yoshihara[d] W. Yasui[b] K. Chayama[a]

[a]Department of Medicine and Molecular Science, Division of Frontier Medical Science, [b]Department of Molecular Pathology, Division of Molecular Medical Science, Programs for Biomedical Research, Graduate School of Biomedical Sciences, Hiroshima University, [c]Department of Endoscopy, Hiroshima University Hospital, Hiroshima, and [d]Health Service Center, Hiroshima University, Higashihiroshima, Japan

Key Words

Gastrointestinal stromal tumor · Nuclear microsatellite instability · Mitochondrial microsatellite instability · BAT26 · D310

Abstract

Objective: Gastrointestinal stromal tumors (GISTs) are the most common mesenchymal tumors of the digestive tract. Nuclear (nMSI) and mitochondrial microsatellite instability (mtMSI) play important roles in tumorigenesis in various organs. The aim of this study was to evaluate the role of nMSI and mtMSI in GISTs. ***Methods:*** Samples from 74 mesenchymal tumors were collected. nMSI and mtMSI were examined by microsatellite assay at BAT26 and D310 mononucleotide repeats in mtDNA, respectively. We compared nMSI, mtMSI and clinicopathologic features, including patient age and sex, tumor location, tumor size, presence of tumor ulceration and presence of distant metastasis, for 51 GISTs for which these data were available. ***Results:*** nMSI and mtMSI were detected in 3 (5%) and 10 (16%) of the 62 GISTs, respectively. There was no significant relationship between nMSI, mtMSI and clinicopathologic features. ***Conclusion:*** These results suggest that mtMSI may play a role, but that nMSI may play little role in the development of GISTs.

Introduction

Gastrointestinal stromal tumors (GISTs), previously classified as smooth muscle tumors, are the most common primary mesenchymal tumors of the gastrointestinal tract [1]. GISTs represent a spectrum of tumors including benign and malignant variants. The immunophenotypic characteristics and genetic profiles of GISTs have clearly distinguished them as a tumor entity separate from other mesenchymal tumors. GISTs are usually positive for the expression of CD34 and c-kit oncoprotein, a transmembrane tyrosine kinase receptor for stem cell factor [2]. Recent studies have shown that mutations of the *c-kit* gene resulting in constitutive activation of the tyrosine kinase play a significant role in tumor pathogenesis [3, 4]. Although *c-kit* mutation was identified in 60–90% of tumors [2, 5], some other molecular alterations may be associated with the development and progression of GISTs [6–9].

Several types of hereditary and sporadic human tumors show high rates of spontaneous mutations due to malfunction of one or more of the mismatch repair genes [10]. Disrupted function of mismatch repair genes manifests itself as nuclear microsatellite instability (nMSI). nMSI has been reported in 80–95% of hereditary nonpolyposis colorectal cancers, in 10–30% of sporadic colorec-

KARGER

Fax +41 61 306 12 34
E-Mail karger@karger.ch
www.karger.com

1015–2008/06/0732–0093$23.50/0

Accessible online at:
www.karger.com/pat

Dr. Shinji Tanaka
Department of Endoscopy, Hiroshima University Hospital
1-2-3 Kasumi, Minami-ku
Hiroshima 734-8551 (Japan)
Tel. +81 82 257 5193, Fax +81 82 257 5194, E-Mail colon@hiroshima-u.ac.jp

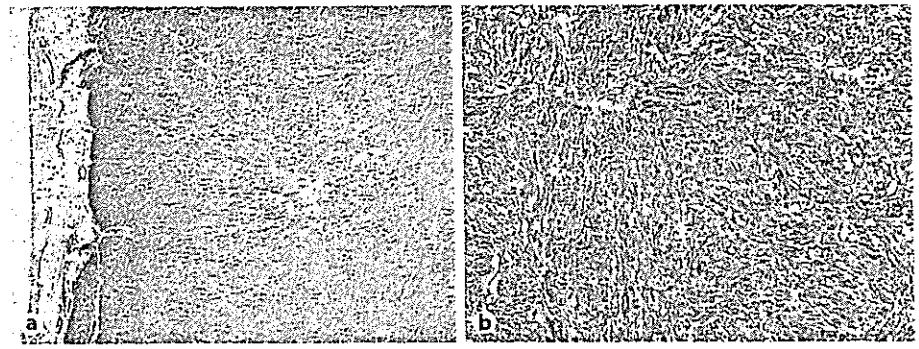

Fig. 1. Representative examples of immunohistochemical staining for KIT. Positive staining was observed. HE. **a** ×40. **b** ×200.

tal cancers and in 15–39% of sporadic gastric cancers [10]. Eukaryote cells not only have a nuclear genome but also cytoplasmic genomes that are compartmentalized in the mitochondria. Mitochcondrial microsatellite instability (mtMSI) is also reported in several types of tumors [11]. However, there are few studies on nMSI and mtMSI in GISTs. We therefore analyzed the nMSI and mtMSI in these tumors in the present study.

Materials and Methods

Tissue Samples

At the Hiroshima University Hospital 74 mesenchymal tumors of the stomach were collected during the period of 1980 through 2000. The mesenchymal tumors were identified as GISTs on the basis of positive immunohistochemical staining for KIT and/or CD34 (fig. 1). With this criterion 62 of the 74 tumors (84%) were identified as GISTs. For each case tumorous and normal tissues were obtained. Clinicopathologic data, including age, sex, tumor location, tumor size, presence of tumor ulceration and presence of distant metastasis, were obtained for 51 of the patients. This study was approved by the local ethics committee (No. I-RIN-HI-45).

Histologic Examination

Four-micron-thick sections were prepared from formalin-fixed, paraffin-embedded specimens. The sections were stained with hematoxylin and eosin (HE) for histologic examination.

DNA Extraction

Ten-micron-thick tissue sections were placed onto glass slides and stained with HE. The sections were then dehydrated in graded ethanol and dried without a cover glass. Tumorous and normal tissues on the slides were scraped up separately with sterile needles. DNA was extracted from the tissues with 20 μl of extraction buffer (100 mM of Tris-HCl, 2 mM of EDTA, pH 8.0, and 400 μl/ml of proteinase K) at 50°C overnight. The samples in tubes were boiled for 7 min to inactivate proteinase K, and 2 μl of aliquots were used for each polymerase chain reaction (PCR) amplification.

Analysis of nMSI

Each tumor was evaluated for nMSI by microsatellite assay with BAT26. The microsatellite assay was performed as described elsewhere [12, 13]. Briefly each 15 μl of reaction mixture containing 10–20 ng of genomic DNA, 6.7 mM of Tris-HCl (pH 8.8), 6.7 mM of EDTA, 6.7 mM of $MgCl_2$, 0.33 μM of labeled primer with [γ-^{32}P]dATP, 0.175 μM unlabeled primer, 1.5 mM of each deoxynucleotide triphosphate and 0.75 U of AmpliTaq Gold DNA polymerase (Perkin-Elmer, Branchburg, N.J., USA) was amplified for 40 cycles as follows: denaturation at 94°C for 30 s, annealing at 55°C for 30 s and strand elongation at 72°C for 30 s. The PCR products were electrophoresed on 6% polyacrylamide-8 M urea-32% formamide gels and autoradiographed overnight at –80°C on Fuji RX film. Tumors with shifted bands at the BAT26 were classified as nMSI [14].

Analysis of mtMSI

A 109-bp fragment containing the D310 repeat of mitochondrial DNA (mtDNA; D-loop region) was amplified [15]. The primer sequences were as follows: 5′-ACAATTGAATGTCTGCACAGCCACTT-3′ for the sense primer and 5′-GGCAGAGATGTGTTTAAGTGCTG-3′ for the antisense primer. Microsatellite assays were performed. Tumors with shifted bands at the D310 repeat were classified as mtMSI [11].

Statistical Analysis

Fisher's exact probability test was used to identify the relationship between D310 mutation and clinicopathologic features. A p value <0.05 was significant.

Results

Clinicopathologic Features of GISTs

Clinicopathologic data including age, sex, tumor location, tumor size, presence of tumor ulceration and presence of distant metastasis were available for 51 cases. All of the 51 GISTs analyzed were located in the stomach and obtained during surgical resection. The male-to-female ratio of the patients was 31:20. The mean age of these patients was 59.0 years (range 20–81). The mean tumor di-

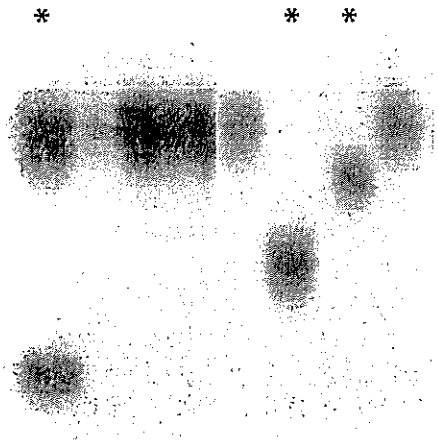

Fig. 2. Representative examples of nMSI. Asterisks indicate a 1-bp deletion of the BAT26 locus.

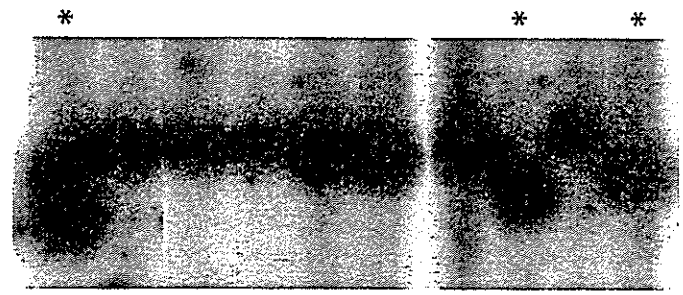

Fig. 3. Representative examples of mtMSI. Asterisks indicate a 1-bp deletion of the D310 mononucleotide repeat.

ameter was 52.1 mm (range 15–200). Thirty-four GISTs (67%) were located in the upper and 17 (33%) in the lower stomach. Forty-two cases (82%) were negative for distant metastasis, and 9 (18%) were positive. Fourteen cases (27%) showed ulceration of the tumor surface and 37 (73%) did not.

Analysis of nMSI

nMSI was detected in 3 of the 62 tumors (5%; fig. 2). Of the 3 positive tumors 1 (33%) showed deletions of 1 bp, 1 (33%) of 3 bp and 1 of 5 bp. We then compared nMSI with the clinicopathologic features in 51 tumors for which clinicopathologic data were available (table 1). No significant relationship was identified between nMSI and each clinicopathologic feature.

Analysis of mtMSI

mtMSI was detected in 10 of the 62 tumors (16%; fig. 3). Of the 10 positive tumors 6 (60%) showed insertions of 1bp, the remaining 4 (40%) deletions of 1bp. We then compared mtMSI with the clinicopathologic features in the 51 tumors for which clinicopathologic data were available (table 2). No significant relationships were identified between mtMSI and each clinicopathologic feature.

Relationship between nMSI and mtMSI

We then examined the relationship between nMSI and mtMSI (table 3). There was no significant relationship between nMSI and mtMSI in GISTs.

Table 1. nMSI in relation to clinicopathologic characteristics of GISTs

Characteristics	nMSI		Frequency of nMSI %	p value
	positive	negative		
Patient age, years				
<60	0	27	0	NS
≥60	2	22	8	
Patient sex				
Male	2	29	6	NS
Female	0	20	0	
Tumor location				
Upper	1	33	3	NS
Lower	1	16	6	
Tumor size (diameter), mm				
<50	1	32	3	NS
≥50	1	16	6	
Tumor ulceration				
Positive	1	13	7	NS
Negative	1	36	3	
Distant metastasis				
Positive	1	8	11	NS
Negative	1	41	2	

NS = Not significant.

Discussion

The molecular pathogenesis of GIST is not fully understood. Alterations in the mismatch repair genes (*hMLH1*, *hMSH2*, *hMSH6*, etc.) are responsible for colorectal, gastric and endometrial tumor formation [10, 11]. Disrupted function of mismatch repair genes manifests itself as nMSI. The cases are classified as having high-frequency MSI (2 or more of 5 microsatellite loci show instability), low-frequency MSI (only 1 of the loci shows instability)

Table 2. mtDNA mutation in relation to clinicopathologic characteristics of GISTs

Characteristics	mtMSI		Frequency of mtMSI %	p value
	positive	negative		
Patient age, years				
<60	4	23	15	NS
≥60	4	20	17	
Patient sex				
Male	7	24	23	NS
Female	1	19	5	
Tumor location				
Upper	5	29	15	NS
Lower	3	14	18	
Tumor size (diameter), mm				
<50	6	27	18	NS
≥50	2	16	11	
Tumor ulceration				
Positive	2	12	14	NS
Negative	6	31	16	
Distant metastasis				
Positive	1	8	11	NS
Negative	7	35	17	

NS = Not significant.

Table 3. Relationship between nMSI and mtMSI in GISTs

	mtMSI		p value
	positive	negative	
nMSI			
Positive	0	3	NS
Negative	8	40	

NS = Not significant.

and microsatellite stable (none of the loci show instability) [16]. As a single test of BAT26 can identify cases positive for high-frequency MSI [13], we evaluated nMSI with microsatellite assay at the BAT26 locus. There are only 2 studies on nMSI in GISTs [17, 18]. One study [18] showed that nMSI was detected in 27% of the tumors and another [17] that no nMSI was found. In the present study nMSI was detected in 4% of the tumors, and it showed that there is no significant relationship between nMSI and clinicopathologic features. These data suggest that nMSI may play little role in the development of GISTs.

The importance of mtDNA in apoptosis has been suggested in several studies[e.g. 19]. Cytochrome c is released from mitochondria, and this is inhibited by the presence of Bcl-2. Cytochrome c interacts with Apaf-1 and procaspase-9 and activates other caspases, leading to apoptosis. This process may be disrupted by mitochondrial dysfunction such as that occurring with mtMSI, and unlimited cell proliferation may result in affected tissues. Tan et al. [20] reported that 22 of 27 breast cancers (81%) had mtMSI. mtMSI was evaluated with alteration of the D-loop region in mtDNA. The region is known to be the start site for replication of the closed, circular mitochondrial genome [21]. Replication of mtDNA begins with the synthesis of the heavy strand with primer RNA, and the 3′ termini of primer RNA have been mapped to CSBs I–III [22]. The identification of alterations in this region indicates the necessity of further research into the mechanisms of late replication and processing of mtDNA in tumors. There have been no studies on mtMSI in GISTs; the present study is the first one. We detected mtMSI in 15% of GISTs, indicating that mtMSI may be involved in the pathogenesis of GISTs. We found no significant relationship between mtMSI and clinicopathologic features. These data suggest that mtMSI may play an important role in the development, but not in the progression of GISTs.

What is the relationship between nMSI and mtMSI, and what is the functional importance of these events for the evolution of cancer cells? Recently Habano et al. [23] reported the existence of an association between nMSI and mtMSI in gastric cancers. However, no such association was found by several other researchers [24, 25]. In addition to these studies no relationship between nMSI and mtMSI has been reported in colorectal, breast and hepatocellular carcinoma [26, 27]. We did not find any relationship between nMSI and mtMSI in GISTs in the present study. NMSI and mtMSI may be independent events in human carcinogenesis.

In conclusion our results suggest that mtMSI may play a role, but that nMSI plays little role in the development of GISTs.

Acknowledgment

We thank Ms. N. Kubota for her technical assistance.

References

1 Miettinen M, Lasota J: Gastrointestinal stromal tumors: definition, clinical, histological, immunohistochemical, and molecular genetic features and differential diagnosis. Virchows Arch 2001;438:1–12.

2 Rubin BP, Singer S, Tsao C, Duensing A, Lux ML, Ruiz R, Hibbard MK, Chen CJ, Xiao S, Tuveson DA, Demetri GD, Fletcher CD, Fletcher JA: KIT activation is a ubiquitous feature of gastrointestinal stromal tumors. Cancer Res 2001;61:8118–8121.

3 Hirota S, Isozaki K, Moriyama Y, Hashimoto K, Nishida T, Ishiguro S, Kawano K, Hanada M, Kurata A, Takeda M, Muhammad Tunio G, Matsuzawa Y, Kanakura Y, Shinomura Y, Kitamura Y: Gain-of-function mutations of c-kit in human gastrointestinal stromal tumors. Science 1998;279:577–580.

4 Nishida T, Hirota S, Taniguchi M, Hashimoto K, Isozaki K, Nakamura H, Hanakura Y, Tanaka T, Takabayashi A, Matsuda H, Kitamura Y: Familial gastrointestinal stromal tumors with germline mutation of the KIT gene. Nat Genet 1998;19:323–324.

5 Taniguchi M, Nishida T, Hirota S, Isozaki K, Ito T, Nomura T, Matsuda H, Kitamura Y: Effect of c-*kit* mutation on prognosis of gastrointestinal stromal tumors. Cancer Res 1999;59:4297–4300.

6 Yamashita K, Igarashi H, Kitayama Y, Ozawa T, Kiyose S, Konno H, Kazui T, Ishikawa S, Aburatani H, Tanioka F, Suzuki M, Sugimura H: Chromosomal numerical abnormality profiles of gastrointestinal stromal tumors. Jpn J Clin Oncol 2006;36:85–92.

7 Blair SL, Al-Refaie WB, Wang-Rodriguez J, Behling C, Ali MW, Moossa AR: Gastrointestinal stromal tumors express ras oncogene: a potential role for diagnosis and treatment. Arch Surg 2005;140:547–548.

8 Nishitani A, Hirota S, Nishida T, Isozaki K, Hashimoto K, Nakagomi N, Matsuda H: Differential expression of connexin 43 in gastrointestinal stromal tumours of gastric and small intestinal origin. J Pathol 2005;206:377–382.

9 Tornillo L, Duchini G, Carafa V, Lugli A, Dirnhofer S, Di Vizio D, Boscaino A, Russo R, Tapia C, Schneider-Stock R, Sauter G, Insabato L, Terracciano LM: Patterns of gene amplification in gastrointestinal stromal tumors (GIST). Lab Invest 2005;85:921–931.

10 Yuen ST, Chan TL, Ho JWC, Chan ASY, Chung LP, Lam PWY, Tse CW, Wyllie AH, Leung SY: Germline, somatic and epigenetic events underlying mismatch repair deficiency in colorectal and HNPCC-related cancer. Oncogene 2002;21:7585–7592.

11 Habano W, Nakamura S, Sugai T: Microsatellite instability in the mitochondrial DNA of colorectal carcinomas: evidence for mismatch repair systems in mitochondrial genome. Oncogene 1998;17:1931–1937.

12 Hiyama T, Yokozaki H, Shimamoto F, Haruma K, Yasui W, Kajiyama G, Tahara E: Frequent *p53* gene mutations in serrated adenomas of the colorectum. J Pathol 1998;186:131–139.

13 Miyoshi E, Haruma K, Hiyama T, Tanaka S, Yoshihara M, Shimamoto F, Chayama K: Microsatellite instability is a genetic marker for the development of multiple gastric cancers. Int J Cancer 2001;95:350–353.

14 Zhou XP, Hoang JM, Li YJ, Seruca R, Carneiro F, Sobrinho-Simoes M, Lothe RA, Gleeson CM, Russell SE, Muzeau F, Flejou JF, Hoang-Xuan K, Lidereau R, Thomas G, Hamelin R: Determination of the replication error phenotype in human tumors without the requirement for matching normal DNA by analysis of mononucleotide repeat microsatellites. Genes Chromosomes Cancer 1998;21:101–107.

15 Sanchez-Cespedes M, Parrella P, Nomoto S, Cohen D, Xiao Y, Esteller M, Jeronimo C, Jordan RC, Nicol T, Koch WM, Schoenberg M, Mazzarelli P, Fazio VM, Sidransky D: Identification of a mononucleotide repeat as a major target for mitochondrial DNA alterations in human tumors. Cancer Res 2001;61:7015–7019.

16 Boland CR, Thibodeau SN, Hamilton SR, Sidransky D, Eshleman JR, Burt RW, Meltzer SJ, Rodriguez-Bigas MA, Fodde R, Ranzani GN, Srivastava S: A National Cancer Institute workshop on microsatellite instability for cancer detection and familial predisposition: development of international criteria for the determination of microsatellite instability in colorectal cancer. Cancer Res 1998;58:5248–5257.

17 Lopes JM, Silva P, Seixas M, Cimes L, Seruca R: Microsatellite instability is not associated with degree of malignancy and p53 expression of gastrointestinal stromal tumours. Histopathology 1988;33:583–585.

18 Fukasawa T, Chong JM, Sakurai S, Koshiishi N, Ikeno R, Tanaka A, Matsumoto Y, Hayashi Y, Koike M, Fukuyama M: Allelic loss of 14q and 22q, *NF2* mutation, and genetic instability occur independently of c-*kit* mutation in gastrointestinal stromal tumor. Jpn J Cancer Res 2000;91:1241–1249.

19 Chinnery PF, Turnbull DM: Mitochondrial DNA and disease. Lancet 1999;354:s17–21.

20 Tan DJ, Bai RK, Wong LJ: Comprehensive scanning of somatic mitochondrial DNA mutations in breast cancer. Cancer Res 2002;62:972–976.

21 Hiyama T, Tanaka S, Shima H, Kose K, Kitadai Y, Ito M, Sumii M, Yoshihara M, Shimamoto F, Haruma K, Chayama K: Somatic mutation of mitochondrial DNA in *Helicobacter pylori*-associated chronic gastritis in patients with and without gastric cancer. Int J Mol Med 2003;12:169–174.

22 Larsson NG, Clayton DA: Molecular genetic aspects of human mitochondrial disorders. Annu Rev Genet 1995;29:151–178.

23 Habano W, Sugai T, Nakamaura S, Uesugi N, Yoshida T, Sasou S: Microsatellite instability and mutation of mitochondrial and nuclear DNA in gastric carcinoma. Gastroenterology 2000;118:835–841.

24 Hiyama T, Tanaka S, Shima H, Kose K, Tuncel H, Ito M, Kitadai Y, Sumii M, Yoshihara M, Shimamoto F, Haruma K, Chayama K: Somatic mutation in mitochondrial DNA and nuclear microsatellite instability in gastric cancer. Oncol Rep 2003;10:1837–1841.

25 Maximo V, Soares P, Seruca R, Rocha AS, Castro P, Sobrinho-Simoes M: Microsatellite instability, mitochondrial DNA large deletions, and mitochondrial DNA mutations in gastric carcinoma. Genes Chromosomes Cancer 2001;32:136–143.

26 Schwartz S, Perucho M: Somatic mutations in mitochondrial DNA do not associate with nuclear microsatellite instability in gastrointestinal cancer. Gastroenterology 2000;119:1806–1807.

27 Fang DC, Fang L, Wang RQ, Yang SM: Nuclear and mitochondrial DNA microsatellite instability in hepatocellular carcinoma in Chinese. World J Gastroenterol 2004;10:371–375.

Pathology International 2006; **56**: 200–205 doi:10.1111/j.1440-1827.2006.01946.x

Original Article

Molecular characteristics of differentiated-type gastric carcinoma with distinct mucin phenotype: LI-cadherin is associated with intestinal phenotype

Junichi Motoshita,[1,2] Hirofumi Nakayama,[1] Kiyomi Taniyama,[2] Keisuke Matsusaki[3] and Wataru Yasui[1]

[1]Department of Molecular Pathology, Hiroshima University Graduate School of Biomedical Sciences, [2]Department of Clinical Laboratory, Pathology Division, National Hospital Organization, Kure Medical Center/Chugoku Cancer Center, Kure and [3]Department of Surgery, Hofu Institute of Gastroenterology, Hofu, Japan

Gastric carcinomas (GC) are classified into four phenotypes on the basis of the mucin expression profile: G type (gastric or foveolar phenotype), I type (intestinal phenotype), GI type (intestinal and gastric mixed phenotype) and N type (neither gastric nor intestinal phenotype). Immunohistochemistry was used to examine the expression of epidermal growth factor receptor (EGFR), E-cadherin, liver–intestine (LI)-cadherin, CD44v9 and p53 and correlation of these molecules with mucin phenotype and tumor stage was evaluated. Overexpression of EGFR and LI-cadherin, reduced expression of E-cadherin and abnormal expression of p53 were observed more frequently in advanced GC than in early GC. Among I-type GC, overexpression of EGFR and reduced expression of E-cadherin were observed more frequently in advanced tumors than in early tumors. Among G-type GC, reduced expression of E-cadherin was significantly associated with advanced tumors. With respect to the relationship between mucin phenotype and expression of cancer-related molecules, overexpression of LI-cadherin was observed more frequently in I-type (12/25, 48.0%) than in G-type (1/14, 7.1%) GC. I-type GC tended to express LI-cadherin more frequently than GI-type GC. These results provide insights into the molecular characteristics of the distinct mucin phenotype of differentiated-type GC and suggest that LI-cadherin may contribute to the biological behavior of I-type GC.

Key words: CD44v9, differentiated-type gastric carcinoma, E-cadherin, epidermal growth factor receptor, immunohistochemistry, liver–intestine-cadherin, mucin phenotype, p53, stomach

Gastric carcinomas (GC) are histologically classified into two major groups. Nakamura *et al.* described the 'differentiated' and 'undifferentiated' types[1] and Lauren described the 'intestinal' and 'diffuse' types based on glandular structure.[2] GC are also classified into four phenotypes on the basis of the mucin expression profile: G type (gastric or foveolar phenotype), I type (intestinal phenotype), GI type (intestinal and gastric mixed phenotype) and N type (neither gastric nor intestinal phenotype).[3–5] However, these classifications are confusing because of the presence of a gastric phenotype with the intestinal type of Lauren or the differentiated type, and of intestinal phenotypic cancers with diffuse structure.[5]

It has been suggested that G-type GC behave more aggressively than I-type GC.[6,7] Tatematsu *et al.* demonstrated, using a rat model, that the proportion of I-type cancer cells increased significantly as gastric lesions progressed from small to large differentiated-type GC.[5] Several distinct genetic differences have been reported between I-type and G-type GC. Mutations of p53 and loss of heterozygosity of the adenomatous polyposis coli (APC) gene occur more frequently in I-type GC than in G-type GC.[8–10] Microsatellite instability and alterations of the p73 gene were shown to be more common in G-type GC than in I-type GC.[11,12] Expression of mucin 2 (MUC2), a marker of intestinal epithelial cells, was associated with DNA methylation of human Mut L homolog 1 (hMLH1) and O^6-methylguanine-DNA methyltransferase (MGMT).[13] However, the molecular mechanism that underlies aggressive behavior of I-type GC remains unclear.

During the progression of GC, multiple genetic and epigenetic alterations accumulate.[14–16] These include overexpression of growth factors/receptors, abnormalities in cell cycle regulators and loss of cell adhesion molecules.[17] Abnormalities in the epidermal growth factor (EGF)/receptor system contribute to the malignant behavior of GC.[15] Loss of E-cadherin is associated with the invasive phenotype of GC.[15,18,19] The expression of CD44v9 is associated not only with tumor advancement but also with recurrence mortality of GC.[15,20] It was recently reported that overexpression of liver–intestine (LI)-cadherin, also known as cadherin-17, is associated with metastasis of GC to the lymph nodes.[21,22] We

Correspondence: Wataru Yasui, MD, PhD, Department of Molecular Pathology, Hiroshima University Graduate School of Biomedical Sciences, 1-2-3 Kasumi, Minami-ku, Hiroshima 734-8551, Japan. Email: wyasui@hiroshima-u.ac.jp

Received 16 August 2005. Accepted for publication 6 December 2005.

reported recently that expression of LI-cadherin correlates with tumor invasion and poor prognosis.[23]

To clarify the molecular characteristics of G-type and I-type differentiated-type GC, we examined the expression of cancer-related molecules such as epidermal growth factor receptor (EGFR), E-cadherin, LI-cadherin, CD44v9 and p53 and evaluated correlation with the mucin phenotypes and tumor stage.

MATERIALS AND METHODS

Tumor samples

Seventy-one samples of differentiated-type GC (38 early GC and 33 advanced GC) from 71 patients were studied. These samples were obtained by surgery at Hiroshima University Hospital or associated facilities between 1996 and 2000. The 71 tumors were classified as Ia ($n = 36$), Ib ($n = 11$), II ($n = 11$), IIIa ($n = 6$), IIIb ($n = 1$) and IV ($n = 6$) according to the post-surgical histopathological tumor, nodes, metastasis classification system (pTNM) classification system.[24] For immunohistochemical staining, tissues were fixed in 10% buffered-formalin and embedded in paraffin. Because written informed consent was not obtained, for strict privacy protection all identifying information was removed from samples prior to molecular expression analysis to protect patient privacy.

Phenotype analysis

GC were classified as G type, I type, GI type or N type according to the results of immunostaining for gastric-type markers (human gastric mucin (HGM) and mucin-recognizing gastric mucous cells (M-GGMC-1)) and intestinal-type markers (MUC2 and CD10) as described previously.[13] In brief, G type consisted of those samples in which >30% of the tumor cells were positive for gastric-type markers and showed little staining of intestinal-type markers. I type consisted of samples in which >30% of the tumor cells were positive for MUC2 or in which >5% of the tumor cells were positive for CD10 and showed little staining of gastric-type markers. GC showing positive staining for both gastric- and intestinal-type markers were classified as GI type, and those with no staining of any of the four markers were classified as N type. Among the 71 GC used in the present study, the mucin phenotype of the 33 advanced GC had been analyzed previously and reported elsewhere.[13]

Immunohistochemistry

Tissue sections (4 μm thick) were prepared from paraffin blocks, and representative sections were immunostained. Immunostaining was done by the immunoperoxidase techniques with a Histofine Simple Stain Kit (Nichirei Biosciences, Tokyo, Japan).[13] Deparaffinized tissue sections were immersed in methanol containing 3% hydrogen peroxide for 15 min to block endogenous peroxidase activity. Sections were microwaved in citrate buffer for 15–45 min to retrieve the antigenicity. Sections were then incubated with primary antibodies against the following antigens: HGM (1:50, NCL-HGM-45M1, Novocastra, Newcastle upon Tyne, UK), M-GGMC-1 (1:50, HIK1083, Kanto Kagaku, Tokyo, Japan), MUC2 (1:200, Ccp58, Santa Cruz Biotechnology, Santa Cruz, CA, USA), CD10 (1:50, NCL-CD10-270, Novocastra), E-cadherin (1:50, HECD-1, Takara Bio, Ohtsu, Japan), LI-cadherin (1:200, sc-6978, Santa Cruz Biotechnology) and p53 (1:100, NCL-p53-DO7, Novocastra), for 1.5 h at 37°C followed by incubation with the secondary antibody for 30 min. Immunocomplexes were then visualized with 3,3′-diaminobenzidine. Sections were counterstained with hematoxylin. For immunostaining of EGFR and CD44v9, a modified immunoglobulin enzyme bridge technique (avidin–biotin peroxidase complex method) was used as described previously.[25] Antibody against EGFR (1:50, NCL-EGFR.113, Novocastra) or antibody against CD44v9 (1:5000, NCL-CD44, Novocastra) was used.

Immunoreactivity was graded according to the number of cells stained and the intensity of the reaction in individual cells. Grades were assigned as follows: EGFR and CD44v9, tumors containing >5% immunoreactive tumor cells were considered positive (overexpression); LI-cadherin, tumors containing >25% immunoreactive tumor cells were considered positive (overexpression);[26] and E-cadherin, tumors containing <5% immunoreactive tumor cells were classified as having reduced expression.[27] For p53, staining was classified as: –, no staining; 1+, <20% of tumor cells stained either intensely or weakly; 2+, 20–50% of tumor cells stained intensely; and 3+, >50% of tumor cells stained intensely. Grades 1+, 2+ and 3+ were regarded as positive and indicated abnormal expression.

Statistics

Fisher's exact test was used for statistical analysis. $P < 0.05$ was regarded as statistically significant.

RESULTS

Mucin phenotypes of gastric carcinoma

The mucin phenotypes and tumor stages of the differentiated-type GC used in the present study and their tumor stage are summarized in Table 1. On the basis of the profile of

Table 1 Mucin phenotypes and tumor stage of differentiated-type GC used in the present study

Stage	G-type	I-type	GI-type	N-type	Total
Early	9	13	9	7	38
Advanced	5	14	9	5	33
TNM					
I, II	12	17	12	12	53
III, IV	2	10	6	0	18
Total	14	27	18	12	71

G-type, gastric or foveolar phenotype; GI-type, intestinal and gastric mixed phenotype; I-type, intestinal phenotype; N-type, neither gastric nor intestinal phenotype; TNM, tumor, nodes, metastases classification.

expression of the four mucin markers, we classified the 38 early GC as nine (23.7%) G-type, 13 (34.2%) I-type, nine (23.7%) GI-type, and seven (18.4%) N-type GC. The mucin phenotypes of the 33 advanced GC (5 (15.2%) G type, 14 (42.4%) I type, 9 (27.2%) GI type and 5 (15.2%) N-type) were reported previously.[13] Most G-type and all N-type GC were of stages I and II, whereas 10 of 27 (37.0%) I-type and six of 18 (33.3%) GI-type GC were of stages III and IV.

Correlation between expression of cancer-related molecules and tumor stage

We first compared the expression of cancer-related molecules between early and advanced differentiated-type GC. Representative staining patterns for EGFR, E-cadherin, LI-cadherin and p53 are shown in Fig. 1, and the overall results are summarized in Table 2. Overexpression of EGFR and LI-cadherin, reduced expression of E-cadherin and abnormal expression of p53 were observed more frequently among advanced GC than among early GC ($P = 0.000056$, $P = 0.00047$, $P = 0.015$ and $P = 0.013$, respectively). These results are consistent with those of previous reports.[15,23,28,29]

We then studied the relation between tumor stage and molecular expression for each mucin phenotype of differentiated-type GC. In general, aberrant expression of EGFR, E-cadherin, LI-cadherin and p53 tended to be more common in advanced tumors than in early tumors regardless of the mucin phenotype, except for LI-cadherin expression in GI-type and p53 expression in GI-type GC. There was no clear trend for CD44v9 expression. The following statistically significant correlations were detected: I-type GC, overexpression of EGFR and reduced expression of E-cadherin were observed more frequently in advanced tumors than in early tumors ($P = 0.0082$ and $P = 0.018$, respectively); G-type GC, reduced expression of E-cadherin was significantly associated with advanced cases ($P = 0.027$); and N-type GC advanced cases frequently showed overexpression of EGFR and LI-cadherin, whereas none of the early cases showed overexpression of these molecules. Because all N-type advanced GC were stage II cancers, no significant association between overexpression of EGFR and LI-cadherin and TNM stage was detected (data not shown).

Table 2 Expression of EGFR, E-cadherin, LI-cadherin, CD44v9 and p53 in differentiated-type GC

Phenotype	Early *n* (%)	Advanced *n* (%)	*P*†	Total *n* (%)
EGFR: overexpression				
G-type	0/8 (0)	2/5 (40.0)	0.13	2/13 (15.4)
I-type	2/13 (15.4)	9/13 (63.2)	0.0082	11/26 (42.3)
GI-type	1/8 (12.5)	3/9 (33.3)	0.58	4/17 (23.5)
N-type	0/7 (0)	3/5 (60.0)	0.045	3/12 (25.0)
Total	3/36 (8.3)	17/32 (53.1)	0.000056	20/68 (29.4)
E-cadherin: reduced expression				
G-type	0/9 (0)	3/5 (60.0)	0.027	3/14 (21.4)
I-type	2/13 (15.4)	11/14 (64.3)	0.018	11/27 (40.7)
GI-type	1/8 (12.5)	4/8 (50.0)	0.28	5/16 (31.2)
N-type	2/7 (28.6)	2/5 (40.0)	1.0	4/12 (33.3)
Total	5/37 (13.5)	18/32 (56.2)	0.00047	23/69 (33.3)
LI-cadherin: overexpression				
G-type	0/9 (0)	1/5 (20.0)	0.36	1/14 (7.1)
I-type	4/13 (30.8)	8/12 (66.7)	0.16	12/25 (48.0)
GI-type	2/8 (25.0)	1/8 (12.5)	1.0	3/16 (18.8)
N-type	0/7 (0)	4/5 (80.0)	0.01010	4/12 (33.3)
Total	6/37 (16.2)	14/30 (46.7)	0.015	20/67 (29.9)
CD44v9: overexpression				
G-type	5/9 (55.6)	3/5 (60.0)	1.0	8/14 (57.1)
I-type	5/13 (38.5)	9/13 (69.2)	0.24	14/26 (53.8)
GI-type	3/9 (33.3)	3/9 (33.3)	1.0	6/18 (33.3)
N-type	3/7 (42.9)	1/5 (20.0)	0.58	4/12 (33.3)
Total	16/38 (42.1)	16/32 (50.0)	0.51	32/70 (45.7)
p53: abnormal expression				
G-type	3/9 (33.3)	3/5 (60.0)	0.58	6/14 (42.9)
I-type	4/13 (30.8)	10/14 (71.4)	0.084	14/27 (51.9)
GI-type	5/9 (55.6)	4/9 (44.4)	1.0	9/18 (50.0)
N-type	1/7 (14.3)	4/5 (80.0)	0.072	5/12 (41.7)
Total	13/38 (34.2)	21/33 (63.6)	0.013	34/71 (47.9)

EGFR, epidermal growth factor receptor; GC, gastric carcinoma; G-type, gastric or foveolar phenotype; GI-type, intestinal and gastric mixed phenotype; I-type, intestinal phenotype; LI, liver–intestine; N-type, neither gastric nor intestinal phenotype.

Early, early GC; advanced, advanced GC.

†Fisher's exact test.

Association between mucin phenotype and expression of cancer-related molecules

Finally, we examined the relation between mucin phenotype and expression of cancer-related molecules. As shown in Table 3, there was a significant association between LI-cadherin expression and mucin phenotype. Overexpression of LI-cadherin was observed more frequently in I-type (12/25, 48.0%) than in G-type (1/14, 7.1%) GC ($P = 0.013$). Moreover, I-type GC tended to express LI-cadherin more frequently than GI-type GC ($P = 0.097$). No such trends were noticed for expression of EGFR, E-cadherin, CD44v9 and p53.

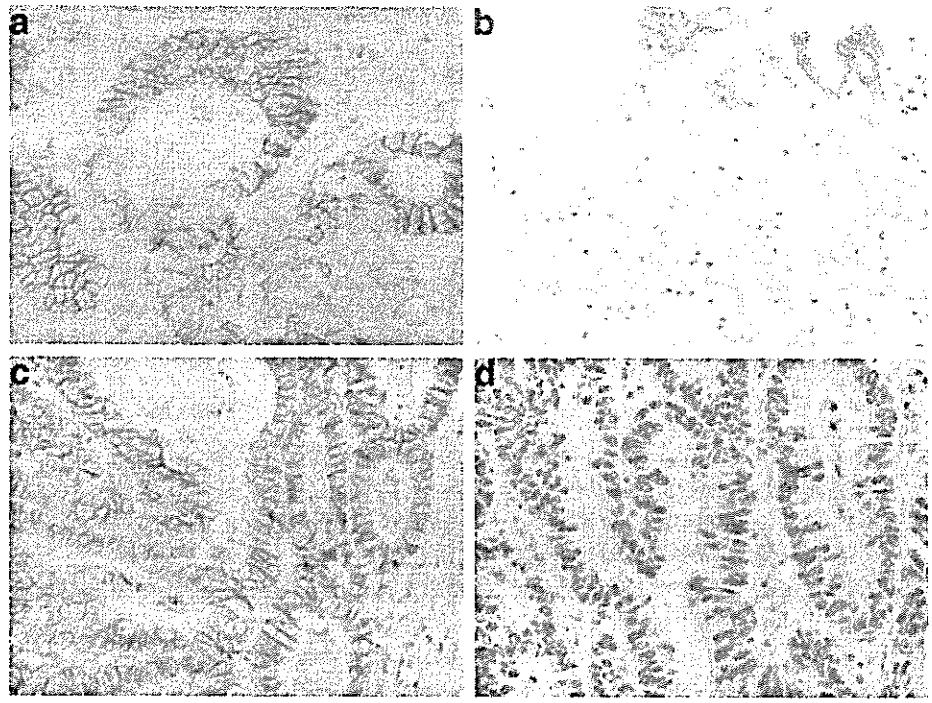

Figure 1 Representative immunohistochemical staining of epidermal growth factor receptor (EGFR), E-cadherin, liver–intestine (LI)-cadherin and p53 in differentiated-type gastric carcinomas (GC). (**a**) In the intestinal and gastric mixed phenotype (GI type) of advanced GC, EGFR is expressed in the cell membrane of many tumor cells. (**b**) In the gastric or foveolar phenotype (G type) of early GC, E-cadherin is expressed in the cell membrane of some tumor cells located superficially, and it is lost in many tumor cells. (**c**) In the intestinal phenotype (I-type) of advanced GC, LI-cadherin is uniformly expressed in cell membrane of most tumor cells. (**d**) In I-type early GC, almost all tumor cells express p53 in their nuclei.

Table 3 Correlation between mucin phenotype and expression of cancer-related molecules

Phenotype			*P*†		
EGFR	E-cadherin	LI-cadherin	CD44v9	p53	
G-type *vs* I-type	0.15	0.30	0.013	0.89	0.83
G-type *vs* GI-type	0.67	0.69	0.60	0.32	0.96
G-type *vs* N-type	0.64	0.67	0.15	0.41	0.74
I-type *vs* GI-type	0.35	0.77	0.097	0.30	0.86
I-type *vs* N-type	0.47	0.93	0.63	0.41	0.81
GI-type *vs* N-type	1.0	0.77	0.42	0.69	0.94

EGFR, epidermal growth factor receptor; GC, gastric carcinoma; G-type, gastric or foveolar phenotype; GI-type, intestinal and gastric mixed phenotype; I-type, intestinal phenotype; LI, liver–intestine; N-type, neither gastric nor intestinal phenotype.
†Fisher's exact test.

DISCUSSION

To clarify the molecular bases of possible biological differences between the mucin phenotypes of GC, we examined expression of representative molecules associated with invasion and metastasis. Our present data for the relation between molecular expression and tumor stage in all of our differentiated-type GC were consistent with the results of previous studies.[15,23,28,29] With respect to specific mucin phenotypes, the expression profiles of certain molecules had statistically significant associations with tumor stage. Among I-type GC, overexpression of EGFR and reduced expression of E-cadherin were detected more frequently in advanced tumors than in early tumors. Among G-type GC, reduced expression of E-cadherin was significantly associated with advanced tumors. Therefore, loss of E-cadherin may be associated with invasion and progression of both G-type and I-type GC, whereas overexpression of EGFR may participate strongly in I-type GC.

Examination of the relationship between expression of specific molecules and mucin phenotypes revealed a significant difference in the expression of LI-cadherin between phenotypes. Overexpression of LI-cadherin was observed more frequently in I-type than in G-type GC, and there was a tendency for I-type GC to express LI-cadherin more frequently than GI-type GC. These results suggest that LI-cadherin may contribute to distinct biological behaviors of I-type GC. LI-cadherin is a structurally unique member of the cadherin superfamily.[30,31] LI-cadherin has only 20 amino acids in the cytoplasmic domain, whereas classical cadherins have a highly conserved cytoplasmic domain that consists of 150–160 amino acids. We previously examined gene expression profiles of GC by serial analysis of gene expression and found that LI-cadherin was one of the most